

# The structure and development of a wing-tip vortex

By WILLIAM J. DEVENPORT, MICHAEL C. RIFE,  
STERGIOS I. LIAPIS AND GORDON J. FOLLIN

Department of Aerospace and Ocean Engineering, Virginia Polytechnic Institute  
and State University, Blacksburg, VA 24061, USA

(Received 10 March 1995 and in revised form 1 November 1995)

Experiments have been performed on the tip vortex trailing from a rectangular NACA 0012 half-wing. Preliminary studies showed the vortex to be insensitive to the introduction of a probe and subject only to small wandering motions. Meaningful velocity measurements could therefore be made using hot-wire probes.

Detailed analysis of the effects of wandering was performed to properly reveal the flow structure in the core region and to give confidence in measurements made outside the core. A theory has been developed to correct mean-velocity profiles for the effects of wandering and to provide complete quantitative estimates of its amplitude and contributions to Reynolds stress fields. Spectral decomposition was found to be the most effective method of separating these contributions from velocity fluctuations due to turbulence.

Outside the core the flow structure is dominated by the remainder of the wing wake which winds into an ever-increasing spiral. There is no large region of axisymmetric turbulence surrounding the core and little sign of turbulence generated by the rotational motion of the vortex. Turbulence stress levels vary along the wake spiral in response to the varying rates of strain imposed by the vortex. Despite this complexity, the shape of the wake spiral and its turbulent structure reach an approximately self-similar form.

On moving from the spiral wake to the core the overall level of velocity fluctuations greatly increases, but none of this increase is directly produced by turbulence. Velocity spectra measured at the vortex centre scale in a manner that implies that the core is laminar and that velocity fluctuations here are a consequence of inactive motion produced as the core is buffeted by turbulence in the surrounding spiral wake. Mean-velocity profiles through the core show evidence of a two-layered structure that dies away with distance downstream.

---

## 1. Introduction

This paper presents measurements that document the structure and development of a tip vortex shed from a conventional wing. Such flows are of engineering importance because they dominate the wakes of lifting vehicles. They are also of scientific interest as examples of turbulent flows dominated by rotation.

There is a large body of literature describing experimental studies of tip vortices. Many of these studies, particularly those concerned with the flow well downstream of the tip, have encountered the problem of wandering. This coherent low-frequency motion of the vortex can lead to large errors in mean velocity and turbulence measurements made with fixed probes. Wandering has been recognized in a number of investigations (e.g. Gasperek 1957; Corsiglia, Schwind & Chigier 1973; Green &

Acosta 1991) and is usually blamed on wind-tunnel unsteadiness. It appears that only Baker *et al.* (1974) have attempted theoretical analysis of its effects.

The early development of tip vortices is revealed in the velocity measurements of McCormick, Tangler & Sherrieb (1968), Chigier & Corsiglia (1971), Mertaugh, Damania & Paillet (1977), Zheng (1992), Chow, Zilliac & Bradshaw (1994) and others. Flow visualizations have also been performed (Francis & Katz 1988; Katz & Bueno Galdo 1989; Engel 1995) as has particle image velocimetry (Green & Acosta 1991; Shekarri *et al.* 1993). The nascent vortex grows quickly with streamwise distance on the suction side of the tip. Its high rate of rotation produces low pressures in its core that accelerate incoming fluid to produce a large axial velocity surplus. Turbulent activity in this region seems to be associated with the separated boundary layer from which the vortex core forms (Chow *et al.* 1994). As the vortex leaves the trailing edge substantial changes occur as it adjusts to the absence of solid boundaries. The core becomes axisymmetric within 2 or 3 chordlengths (Accardo, Cenedese & Cioffi 1984; Green & Acosta 1991) and the axial velocity surplus usually reverses, becoming a deficit. Some authors show the almost immediate formation of a deficit (e.g. Stinebring, Farell & Billet 1991; Shekarri *et al.* 1993) whereas others show a surplus persisting further downstream (e.g. Thompson 1975; Green & Acosta 1991). The vortex path may develop a kink just downstream of the trailing edge (Chigier & Corsiglia 1971; Green & Acosta 1991; Engel, 1995) produced by interaction with secondary structures shed from the tip. Velocity fluctuations in the vortex core can be intense here (Green & Acosta 1991; Chow *et al.* 1994) due to unsteadiness as well as turbulence. Chow *et al.* (1994) show the turbulence to be rapidly stabilized by the rotation of the core downstream of the trailing edge, but Green & Acosta (1991) show significant unsteadiness persisting up to 10 chordlengths downstream. Turbulence is also found in the rest of the wake which, once shed from the wing, begins its roll-up into a spiral structure around the core (Mertaugh *et al.* 1977; Stinebring *et al.* 1991; Chow *et al.* 1994; Zheng 1994).

The development of the vortex further downstream has been documented by several fixed-probe studies, but few attempt to verify the absence of wandering and none try to correct for its effects, making it difficult to draw firm conclusions. Of these measurements, Singh & Uberoi's (1976) appear least affected by wandering. These measurements, made up to 80 chordlengths downstream, show velocity fluctuations to be strongest in a ring surrounding the core. The vortex was shed from a laminar flow wing, however, and had a large destabilizing axial velocity deficit (Mayer & Powell 1992) that is not found in most tip vortices. Perhaps the most useful studies in this region have been performed in free flight (e.g. McCormick *et al.* 1968; Bisgood, Maltby & Dee 1971; Panton, Oberkampf & Soskic 1980), by scanning probes through the vortex (e.g. Corsiglia *et al.* 1973; Ciffone & Orloff 1975) or through flow visualization (e.g. Lezius 1974; Sarpkaya 1992). The consensus of much of the scanning and free-flight work, established in the papers of Ciffone (1974) and Iversen (1976) is that tip vortices show little growth or decay over the first 20 or more spans downstream of the wing (i.e. for about as long as the vortex develops independently of its twin shed from the opposite wing tip). Iversen attributes this to the action of a non-equilibrium turbulence structure, on the basis of earlier turbulence model calculations by Donaldson (1972) and Baldwin, Chigier & Sheaffer (1973). The presence of turbulence, or at least significant unsteadiness, in the vortex core would appear to be consistent with the flow visualizations of Sarpkaya (1992) but appears at odds with low turbulence levels measured in an aircraft tip vortex by Panton *et al.* (1980) and full-scale flow visualizations, such as those of Huffaker, Jelalian & Thompson (1970) and

Garodz (1971) which suggest a laminar-like structure. Laminar flow could explain the very slow decay, and appears plausible given the stability calculations of Mayer & Powell (1992). A laminar core is also suggested by recent simulations (Ragab & Sreedhar 1995; Ragab 1995) and turbulence calculations (Zeman 1995).

While there have been very few reliable turbulence measurements in a tip vortex beyond the tip region, such measurements have been made on trailing vortices generated by split wings. Split-wing vortices appear less susceptible to wandering (although not immune, see Vogel, Devenport & Zsoldos 1995) and are thus more easily measured. Turbulence stress measurements have been made in split-wing vortices by Phillips & Graham (1984) and Bandyopadhyay, Stead & Ash (1991), among others. Both of these studies show velocity fluctuations to be near maximum in the vortex core. At the same time, Phillips & Graham's data show almost no discernable diffusion of the core (unless a strong jet or wake is superimposed) and Bandyopadhyay *et al.*'s visualizations and velocity traces suggest that the core is relaminarizing. The large stresses in the core may therefore indicate the presence of unsteadiness in the core not associated with turbulent mixing (or wandering). Core velocity spectra and flow visualization analysis by Bandyopadhyay *et al.* suggest that some of this unsteadiness may have a coherent wave-like form. While these results are interesting, it should be borne in mind that tip and split-wing vortices can have a quite different turbulence structure. Specifically, split-wing vortices are formed by the merger of two tip vortices, the merging process producing a large region of roughly axisymmetric turbulence around the core that is absent from a tip vortex (Smits & Kummer 1985; Zsoldos & Devenport 1992). A comparison of the turbulence structure of split-wing and tip vortices generated under like conditions may be made by comparing the results of Zsoldos & Devenport (1992) or Vogel *et al.* (1995) with those of the present paper.

Despite much work there is obviously a lot missing from our understanding of tip vortices beyond a few chordlengths downstream of the wing. There have been no measurements of the cross-sectional turbulent structure outside the core and few if any low-uncertainty mean flow or time-average turbulence measurements inside, leaving turbulence modellers little to go on. Considering its universal nature, there has also been surprisingly little attention paid to characterizing the wandering problem and quantitatively accounting for its effects.

It is the objective of the present investigation to provide new understanding of tip vortex flows in this region. With the above backdrop our approach has been to study the vortex shed from a conventional wing tip and, despite wandering, to do it using fixed hot-wire probes, since only these can provide the necessary statistical and spectral information. Unlike many previous investigations, however, we have gone to some lengths to analyse and quantify the effects of vortex wandering. We have been able to reverse its effects on mean-velocity measurements and have used spectral decomposition to separate its velocity fluctuations from those produced by turbulence. This approach has yielded, for the first time, clear views of the time-averaged turbulence structure of these flows.

This paper is organized as follows. We begin with descriptions of the apparatus and instrumentation (§2) and of the analysis of the effects of wandering (§3). The presentation of results and discussion (§4) begins with a description of the overall form of the vortex and then examines in detail the flow structure inside and outside the core region. The main findings are that the core of the vortex is laminar and therefore develops very slowly, and that the turbulence structure in the wake spiral reaches a self-similar form.

## 2. Apparatus and instrumentation

Experiments were performed in the Virginia Tech Stability Wind Tunnel. This facility has a test section of square cross-section  $1.83 \times 1.83$  m and length 7.33 m. Flow in the empty test section is closely uniform with a turbulence intensity of less than 0.1 % (low-frequency cut-off  $\approx 2$  Hz, Choi & Simpson 1987). A slight favourable streamwise pressure gradient  $dC_p/dx = -0.3\% \text{ m}^{-1}$  exists in the test section owing to boundary layer growth.

A rectangular-planform NACA 0012 wing with a 0.203 m chord ( $c$ ) and blunt tip was used to generate the vortices. It was mounted vertically as a half-wing at the centre of the upper wall of the test section entrance with 0.879 m protruding into the flow (figure 1). For most of the measurements the boundary layer on the wing was tripped using 0.5 mm diameter glass beads glued in a random pattern between the 20 % and 40 % chord locations. Average density was  $200 \text{ beads cm}^{-2}$ . Some measurements were also made using a more severe trip extending from the 0 % to 40 % locations, and some were made with no trip at all. To judge the effectiveness of the trips, boundary layers at the wing trailing edge were measured using single hot wires (Devenport, Glegg & Sharma 1992). These data show fully turbulent boundary layers except on the pressure side when no trip was used. The boundary layer here appeared transitional. Typical boundary layer properties are summarized in table 1.

A miniature four-sensor hot-wire probe consisting of two orthogonal X-wire arrays (Auspex Corp. AVOP-4-100, figure 2) was used for velocity measurements in the vortices. It has  $5 \mu\text{m}$  tungsten sensors 0.8 mm in length and a measurement volume of some  $0.5 \text{ mm}^3$ . This type of probe, more normally associated with vorticity measurements (e.g. Kovasznay 1954), was chosen after an initial study (Devenport *et al.* 1992) showed it to be better than standard triple and X-array probes for trailing vortex measurements. The triple-wire probe was found to be very sensitive to gradient errors of the type found in vortices, axial velocity measurements being contaminated (up to 10 %) by the streamwise vorticity. The X-array probe also displayed some sensitivity to streamwise vorticity and produced large uncertainties in Reynolds stress measurements because the velocity components were not measured simultaneously. The 4-sensor probe, being capable of simultaneous 3-component measurements from a relatively compact measurement volume, appeared to overcome both of these problems. Note that 4-sensor probes, which can suffer serious problems in boundary layers (Vukoslavčević & Wallace 1981), are well suited to wake flows because they contain only weak axial velocity gradients.

Each of the hot-wire sensors was operated separately using a Dantec 56C17/56C01 anemometer unit. Anemometer outputs were read by an IBM AT compatible computer through an Analogic 12 bit HSDAS-12 A/D converter buffered by four  $\times 10$  buck-and-gain amplifiers. The dynamic response of all four channels of the system was measured separately using the method of Wood (1975) and found to be adequate to well over 20 kHz. A traversing gear mounted in the wind tunnel allowed horizontal and vertical positions of the probe to be controlled from the computer. A probe holder (figure 2) positioned the tip of the probe well upstream of the traverse gear. Rods were used to offset the probe from the holder so that the holder did not have to be placed in or near the vortex core for the probe to be positioned there. The probe was held parallel to the free-stream direction for all velocity measurements since previous studies (see Appendix A) indicated that pitching or yawing the probe in the vortex would lead to probe interference.

The probe was calibrated separately for velocity and angle response. Velocity

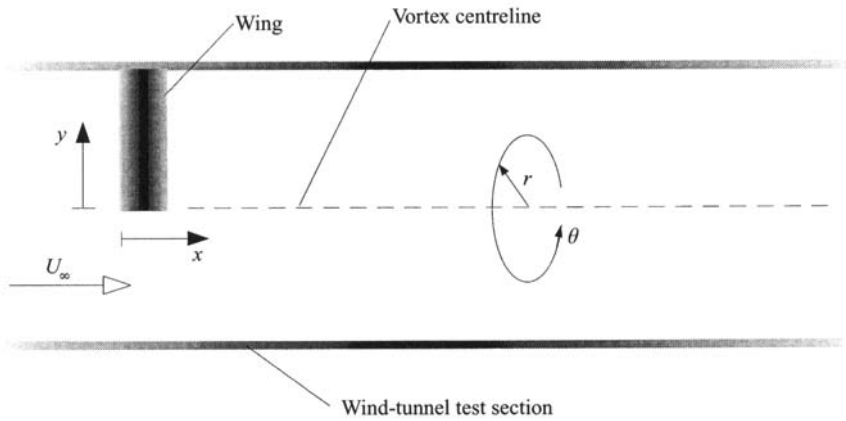


FIGURE 1. Schematic of the wind-tunnel test section showing coordinate systems. The direction of coordinate  $z$  is out of the paper.

	Pressure side	Suction side
$\delta/c \times 100$	4.35	6.22
$\delta^*/c \times 100$	0.99	1.61
$\theta/c \times 100$	0.58	0.87
$Re_\theta$	2900	4355

TABLE 1. Boundary layer properties at the wing trailing edge for the baseline flow. Chord  $Re = 530\,000$ , 20–40% trip,  $5^\circ$  angle of attack,  $y/c = 1.2$

calibrations were performed in the wind-tunnel free stream. Cooling velocities were determined using a Pitot static probe accounting for the effective angle of each of the sensors and the local flow direction at the calibration position, the latter being determined in advance using a seven-hole yaw probe. King's law was used to curve fit calibrations to an accuracy of better than 1%. To calibrate the angle response a method similar to that of Mathioudakis & Breugelmans (1985) was used. In this method the probe is placed in the potential core of a uniform jet of known flow direction and velocity equal to the wind-tunnel free-stream velocity. The cooling velocities are then measured as the probe is pitched and yawed over all likely angle combinations from  $+45^\circ$  to  $-45^\circ$ . At each angle combination, standard X-array response equations (e.g. Tutu & Chevray 1975) are used to extract rough estimates of  $U$  and  $V$  from the cooling velocities of one pair of sensors and  $U$  and  $W$  from the other (figure 2). After averaging the two  $U$  estimates (to minimize the influence of axial vorticity) the quantities  $V/Q$ ,  $W/Q$  and  $Q$  are calculated, where  $Q = (U^2 + V^2 + W^2)^{1/2}$ . Look up tables of the errors in these estimates as a proportion of  $Q$  are then constructed by comparing them with true values inferred from the pitch and yaw angles. Interpolations on these tables are then used to correct instantaneous estimates of  $V/Q$ ,  $W/Q$  and  $Q$  obtained during a measurement. Residual errors, evaluated by reprocessing the angle calibration data, were small. Repeatability was also found to be good. The angle calibration appeared to be a strong function only of the prong geometry.

This approach is much more accurate than using only standard angle response equations and avoids several difficulties normally associated with the accurate solution of those equations. The calibration process also reveals the acceptance cone of the



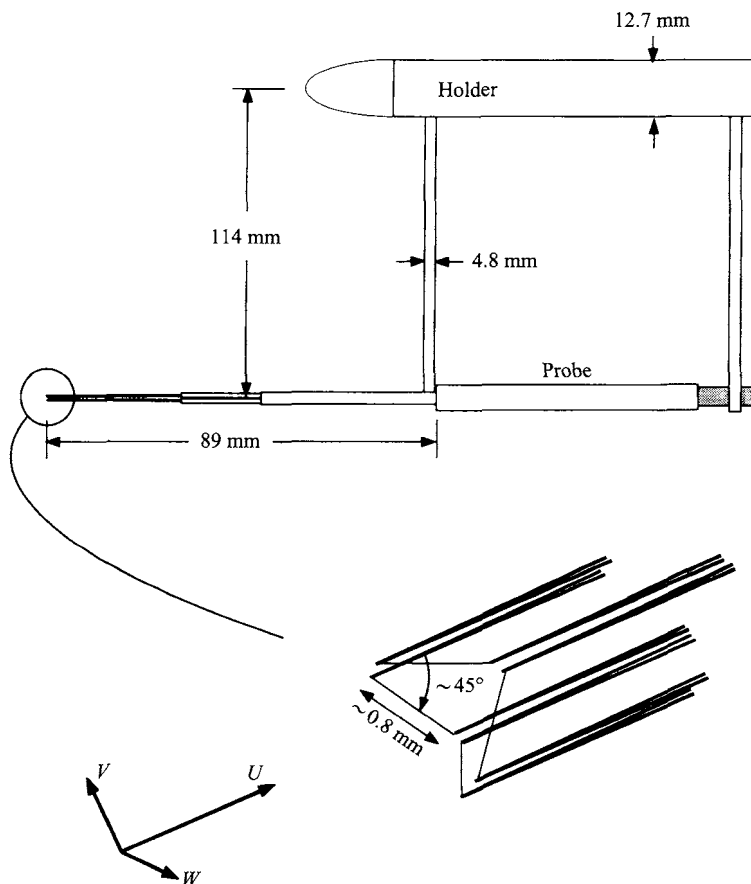


FIGURE 2. Schematic of the hot-wire probe and support.

probe (the region within which a single-valued relationship between the cooling velocities and velocity components can be established) thereby preventing non-uniqueness problems. One advantage of the method over others in which look up tables are used (e.g. Leuptow, Breuer & Haritonidis 1988; Browne, Antonia & Chua 1989; Döbbeling, Lenze & Leukel 1990) is that sophisticated interpolation is not required because the corrections vary only slowly over most of the acceptance cone. One possible drawback is the assumption that the angle calibration is independent of velocity. In the present flows, however, absolute velocity variations were small (typically  $< \pm 15\%$ ) and angle calibrations performed over a range of speeds indicated negligible dependence on velocity over this range.

Hot wires offer some desirable characteristics of measuring tip vortices. They give continuous, low-noise signals and are well suited to the measurement of velocity spectra – important if vortex wandering and other inactive motions are to be separated from turbulence. They are also capable of measuring the low turbulence levels one expects and readily give the statistical turbulence information used by turbulence modelers. Hot wires are intrusive, however, and tip vortices have a reputation for being unusually sensitive to probe interference. Establishing the lack of interference was therefore an important prerequisite of the present study. The results of this work, described in Appendix A, show no evidence of interference at any of the measurement conditions studied.

### 3. Wandering

A second problem that must be addressed in using a fixed probe is wandering – the slow side-to-side movement of the vortex core that seems to be a universal feature of wind-tunnel-generated vortices. Wandering may be self-induced or a consequence of free-stream unsteadiness but in either case its most significant effect is to obscure important flow details. It is so far separated from turbulent motions in terms of frequency that its influence on vortex development is almost certainly negligible.

In the past there has been little attempt to precisely quantify wandering or accurately estimate the errors it produces. Without such estimates it is very difficult to interpret measurements made using fixed probes in and around tip vortex cores. Part of the reason for this state of affairs may be the perception that the effects of wandering are overwhelming and irreversible. While this is certainly the case when the wandering amplitude is many times the core diameter (e.g. Corsiglia *et al.* 1973) we have found that it is not so when the amplitude is much smaller, as in the present experiment. Below we develop a mathematical description of the effects of wandering, the results of which provide methods for determining the amplitude of wandering, for estimating its effects, and for reversing those effects.

Consider the situation shown in figure 3 which shows a cross-section through a tip vortex subject to coherent wandering motions. What we desire are velocity measurements in a frame of reference that moves with the wandering. What we have are measurements in a fixed frame. To deduce the former from the latter we must assume that the wandering is independent of any turbulent motion and that velocities associated with the wandering movement itself are negligible in comparison to those generated by the vortex.

Figure 3 shows three points: the origin, defined as the location of the vortex centre averaged over its coherent motions; the current location of the vortex centre ( $y_v, z_v$ ) and the location of the probe ( $y_p, z_p$ ). Consider the velocity field generated by the vortex in its current location, specifically the Cartesian components  $U, V, W$  sensed by the probe. These are functions of  $y$  and  $z$ , the position of the probe relative to the current vortex centre, e.g.

$$U(y, z) = U(y_p - y_v, z_p - z_v). \quad (1)$$

Because of the wandering motions the absolute position of the vortex centre changes. Over a long period of time we can describe the vortex position using a probability density function (p.d.f.),

$$p = p(y_v, z_v). \quad (2)$$

So, over a long period of time the probe will measure mean velocities given by

$$U_m(y_p, z_p) = \int_{-\infty}^{\infty} \int_{-\infty}^{\infty} p(y_v, z_v) U(y_p - y_v, z_p - z_v) dy_v dz_v, \quad (3)$$

with like expressions for  $V$  and  $W$ , and apparent Reynolds stresses given by

$$\overline{uw}_m(y_p, z_p) = \int_{-\infty}^{\infty} \int_{-\infty}^{\infty} p(y_v, z_v) U(y_p - y_v, z_p - z_v) V(y_p - y_v, z_p - z_v) dy_v dz_v - U_m V_m, \quad (4)$$

with like expressions for  $\overline{u_m^2}, \overline{v_m^2}, \overline{w_m^2}, \overline{vw}_m$  and  $\overline{uw}_m$ . (As is common practice, we refer to the mean square velocity fluctuations and correlations as stresses, the multiplying density having been dropped for brevity.) Relations similar to equation (3) may be written for any quantity linearly related to the Cartesian velocity components, e.g. vorticity. Equation (3) was first derived by Baker *et al.* (1974).

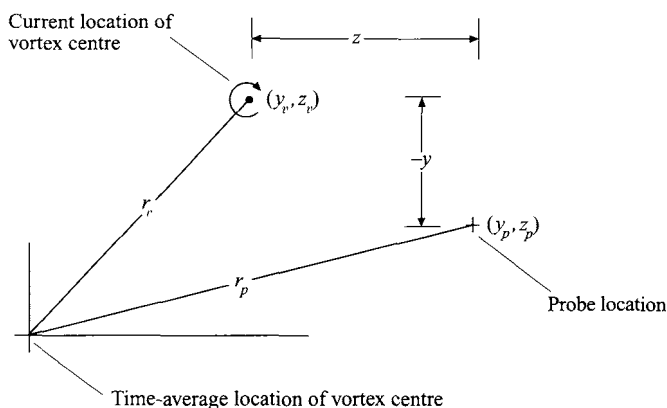


FIGURE 3. Coordinate system and definition of symbols for wandering analysis.

Our objective here is to reverse the smoothing process implied by equation (3), i.e. to determine the true mean velocity field in terms of that measured, and then compute the Reynolds stress contributions given in equation (4). In principle this is straightforward since equation (3) is the convolution of  $p$  with  $U$  and so can be inverted using Fourier transforms. Numerical application of such a procedure is, however, impractical. A more workable approach is to use equation (3) to reveal analytically the effects of wandering on specific velocity fields and then use these results to determine corrections. We consider below two such solutions. The first, for a  $q$ -vortex, gives simple rules of thumb for estimating the wandering amplitude and the magnitude of its effects on measured core parameters. The second, for a general vortex, provides a comprehensive method for correcting mean velocity profiles for the effects of wandering and for determining its effects upon turbulence stress fields.

### 3.1. Solution for a $q$ -vortex

Several previous studies of trailing vortices (e.g. Dosanjh, Gasperek & Eskinazi 1962; Hoffman & Joubert 1963; Phillips & Graham 1984) report mean tangential and axial velocity profiles that, in the vicinity of the core, are similar to the laminar  $q$ -vortex solution of Batchelor (1964), i.e.

$$V_\theta = V_{\theta 1} (1 + 0.5/\alpha) \frac{r_1}{r} \left[ 1 - \exp\left(-\alpha \frac{r^2}{r_1^2}\right) \right] \quad (5)$$

$$\text{and} \quad U = U_d \exp\left(-\alpha \frac{r^2}{d^2}\right), \quad (6)$$

where  $r^2 = y^2 + z^2$ ,  $\alpha = 1.25643$  and  $V_{\theta 1}$ ,  $U_d$ ,  $r_1$  and  $d$  are respectively the measured peak tangential velocity, centreline axial velocity (relative to free stream), core radius and radial scale of the axial profile. Imagine such a vortex subject to wandering motions being measured with a fixed probe. If we assume Gaussian isotropic wandering of r.m.s. amplitude  $\sigma$ , i.e.

$$p(y_v, z_v) = \frac{1}{2\pi\sigma^2} \exp\left(-\frac{y_v^2 + z_v^2}{2\sigma^2}\right), \quad (7)$$

then we may determine the measured flow field analytically. In the case of the tangential velocity this is done by expressing  $V_\theta$  in terms of a Cartesian component, say  $V = V_\theta z/r$ , substituting it and equation (7) into equation (3) and performing the



integration. This is most easily done in the Fourier domain (see Monaghan & Humble 1993 for the required transform) and yields, after converting back to tangential velocity,

$$V_{\theta m} = V_{\theta 1}(1 + 0.5/\alpha) \frac{r_1}{r_p} \left[ 1 - \exp \left( -\alpha \frac{r_p^2}{r_1^2 + 2\alpha\sigma^2} \right) \right], \quad (8)$$

where  $r_p^2 = y_p^2 + z_p^2$ . This is still a  $q$ -vortex profile but with a larger core radius and lower peak tangential velocity. The ratio between the true core radius and that measured is

$$r_1/r_{1m} = (1 - 2\alpha\sigma^2/r_{1m}^2)^{1/2}. \quad (9)$$

The ratio between the true peak tangential velocity and that measured is

$$V_{\theta 1}/V_{\theta 1m} = r_{1m}/r_1 \quad (10)$$

which implies that the true core circulation is measured despite wandering.

Proceeding in the same way we find that the measured axial velocity field is still Gaussian,

$$U_m = U_{Dm} \exp \left( -\alpha \frac{r_p^2}{d_m^2} \right) \quad (11)$$

but with a smaller centreline velocity

$$U_{Dm} = \frac{U_D}{1 + 2\alpha\sigma^2/d^2} \quad (12)$$

and a larger radial scale  $d_m$ , the ratio between  $d$  and  $d_m$  being the same as that between  $r_1$  and  $r_{1m}$ .

Equations (9), (10) and (12) show that the consequences of wandering can be serious. Wandering of r.m.s. amplitude equivalent to 50% of the measured core radius will result in a 64% overestimate of core radius, and an equivalent underestimate of peak tangential velocity. Similar errors are predicted for the axial velocity. Some comfort might be taken from the fact that form of the profiles is unaltered. However, this is not a general result but a consequence of the special invariance of Gaussian functions under convolution (the  $q$ -vortex tangential velocity field implies a Gaussian axial vorticity field). In fact, it can be proved (see Appendix B) that with Gaussian wandering any axial vorticity or velocity field will smooth toward a Gaussian form. The velocity field of any vortex will therefore appear as a  $q$ -vortex given sufficient wandering. Any apparent universality of the  $q$ -vortex form may therefore be a symptom of the universality of vortex wandering rather than of any underlying physical structure.

Equations (9), (10) and (12) can be used to estimate the effects of wandering upon measured vortex parameters. To apply them, however, it is necessary to have the r.m.s. amplitude of vortex wandering  $\sigma$ . This may be obtained from mean-square tangential velocity measured at the core centre,  $v_{\theta m}^2(0,0)$  (inferred from a  $v$  or  $w$  measurement), if we assume that this is entirely generated by vortex wandering. Dividing the square root of  $v_{\theta m}^2(0,0)$  by the measured tangential velocity gradient at the core centre one obtains a first estimate of the wandering amplitude  $\sigma_m$ . Assuming isotropic Gaussian wandering and a  $q$ -vortex mean-velocity field it is possible to derive the following implicit relationship between this estimate and the true value:

$$\frac{\sigma_m^2}{r_{1m}^2} = \frac{(r_1^2/\sigma^2 + 2\alpha)}{2\alpha^2} \ln \left( \frac{2\alpha\sigma^2/r_1^2 + 1}{(4\alpha\sigma^2/r_1^2 + 1)^{1/2}} \right). \quad (13)$$

It is simple to show that in absolute terms (i.e. not normalized on  $r_1$ ) the actual wandering amplitude will always be less than the estimate.

### 3.2. General solution method

In general, as in the present experiments, tip vortices do not have  $q$ -vortex velocity distributions and their wandering may not be isotropic. A broader method is therefore needed if the true velocity fields and wandering characteristics of real vortices are to be accurately determined from fixed probe measurements. This method avoids the impractical numerical inversion of equation (3) by making two simplifying assumptions.

First we assume that flow in the vicinity of the vortex core is axisymmetric and that the true axial velocity and vorticity fields here may be accurately described by series of the form

$$g(y, z) = \sum_{i=1}^n A_i \exp\left(-\frac{y^2 + z^2}{a_i^2}\right), \quad (14)$$

where  $A_i$  and  $a_i$  are constant coefficients and, in the case of axial velocity, the free-stream velocity has been subtracted. This series cannot describe arbitrary functions, but it is well suited to the bell-shaped velocity and vorticity distributions of vortices. The series and following method could be generalized by incorporating additional coefficients to shift the origins of  $y$  and  $z$  but we have found this unnecessary. Our interest in the vorticity comes out of a desire to obtain the tangential velocity field. If  $g(y, z)$  is used to represent vorticity ( $= (1/r)(\partial r V_\theta / \partial r)$ ) this implies a tangential velocity

$$V_\theta(y, z) = \sum_{i=1}^n \frac{B_i}{r} \left[ 1 - \exp\left(-\frac{y^2 + z^2}{a_i^2}\right) \right], \quad (15)$$

where  $B_i = A_i a_i^2 / 2$ .

Secondly, we assume a non-isotropic Gaussian form for the p.d.f. of vortex position

$$p(y_v, z_v) = \frac{1}{2\pi\sigma_y\sigma_z(1-e^2)^{1/2}} \exp\left[\frac{-1}{2(1-e^2)}\left(\frac{z_v^2}{\sigma_z^2} + \frac{y_v^2}{\sigma_y^2} - \frac{2y_v z_v}{\sigma_y\sigma_z}\right)\right], \quad (16)$$

where  $\sigma_y$  and  $\sigma_z$  are the r.m.s. amplitudes of wandering and  $e$  is the correlation coefficient. Since  $\sigma_y$ ,  $\sigma_z$  and  $e$  are determined as part of the problem, this assumption is not very critical. Using, for example, a uniform distribution in place of the Gaussian was found to produce differences in corrections for wandering that were smaller than the uncertainty in the rest of the method.

Given these assumptions the problem at hand is to determine  $A_i$ ,  $a_i$ ,  $\sigma_y$ ,  $\sigma_z$  and  $e$  from measurements made in the vortex in the presence of wandering. Substituting equations (14) and (16) into (3) and performing the integration analytically we obtain

$$g_m(y_p, z_p) = \sum_{i=1}^n \frac{A_i a_i^2}{E_i^{1/2}} \exp\left(\frac{-1}{E_i} (y_p^2 [2\sigma_z^2 + a_i^2] + z_p^2 [2\sigma_y^2 + a_i^2] - 4y_p z_p e \sigma_y \sigma_z)\right), \quad (17)$$

where  $E_i = (2\sigma_y^2 + a_i^2)(2\sigma_z^2 + a_i^2) - 4e^2\sigma_y^2\sigma_z^2$ . Consider now a cut through this distribution along the  $z$ -axis as would be measured when taking a profile through the average vortex centre location:

$$g_m(0, z_p) = \sum_{i=1}^n \frac{A_i a_i^2}{E_i^{1/2}} \exp(-z_p^2 [2\sigma_y^2 + a_i^2] / E_i) = \sum_{i=1}^n C_i \exp(-z_p^2 / c_i^2) \quad (18)$$

say. In the case of the axial velocity, if the coefficients  $C_i$  and  $c_i$  are determined by fitting the measured profile, then the coefficients of the true axial velocity distribution

$A_i$  and  $a_i$  may be obtained by comparing terms in equation (18). After some algebraic manipulation this gives

$$\left. \begin{aligned} a_i^2 &= \frac{1}{2}c_i^2 - \sigma_y^2 - \sigma_z^2 + \frac{1}{2}[(2\sigma_y^2 + 2\sigma_z^2 - c_i^2)^2 - 16\sigma_y^2\sigma_z^2(1-e^2) + 8\sigma_y^2c_i^2]^{1/2}, \\ A_i &= C_i E_i^{1/2}/a_i^2, \end{aligned} \right\} \quad (19)$$

where positive square roots are taken.

Consider now the case of the axial vorticity. The wandered vortex is no longer axisymmetric so the vorticity is equal to  $(1/r)(\partial r V_\theta/\partial r) - (1/r)(\partial V_r/\partial \theta)$ , making the tangential velocity difficult to compute. However, the second term will be small except in extreme circumstances so we calculate the tangential velocity by ignoring it:

$$V_{\theta m}(0, z_p) = \sum_{i=1}^n \frac{D_i}{z_p} \left[ 1 - \exp\left(\frac{-z_p^2}{c_i^2}\right) \right], \quad (20)$$

where  $D_i = C_i c_i^2/2$ . If the coefficients  $D_i$  and  $c_i$  are now obtained by fitting a measured profile, the coefficients of the true tangential velocity field  $B_i$  and  $a_i$  are given by equation (19) and

$$B_i = D_i(2\sigma_y^2 + a_i^2)/E_i^{1/2}. \quad (21)$$

The above relations provide a method for estimating the true vortex velocity distribution given  $\sigma_y$ ,  $\sigma_z$  and  $e$ . Determining these is straightforward if we have a measurement of the intensity of cross-flow velocity fluctuations at the core centre produced by wandering, specifically,  $\overline{v_m^2}$ ,  $\overline{w_m^2}$  and  $\overline{vw_m}$ . In many situations (as in the present flows) these statistics may be obtained from the raw velocity signal since this is usually dominated by wandering. In situations where turbulent fluctuations are also important, low-pass filtering may be necessary. We begin by assuming values for  $\sigma_y$ ,  $\sigma_z$  and  $e$ . These and the above curve fits to the measured velocity profiles  $U_m$  and  $V_{\theta m}$  are then used to estimate the true velocity field for the vortex via equations (19) and (21). With this estimate and the assumed wandering amplitudes, equation (4) is used to compute the apparent stresses  $\overline{v_m^2}$ ,  $\overline{w_m^2}$  and  $\overline{vw_m}$  at the core centre. In general these will not agree with the measured values so  $\sigma_y$ ,  $\sigma_z$  and  $e$  are adjusted and the procedure repeated until they do. If  $\sigma_y$  and  $\sigma_z$  are adjusted by writing

$$\sigma_{y_{new}}^2 = \sigma_{y_{old}}^2 \overline{w_{m_{meas}}^2} / \overline{w_{m_{calc}}^2}, \quad \sigma_{z_{new}}^2 = \sigma_{z_{old}}^2 \overline{v_{m_{meas}}^2} / \overline{v_{m_{calc}}^2} \quad (22)$$

and  $e$  is recalculated by requiring that the principle axes of the apparent stresses be the same as those of the wandering (as they must), then convergence is achieved within a few iterations.

This technique yields estimates of the true velocity field of the vortex and the wandering amplitudes from measured mean velocity profiles and the intensity of velocity fluctuations of the core centre generated by wandering. With these results equations (3) and (4) may be applied to compute the full mean velocity and apparent stress fields that should be measured in the presence of the wandering. The former, when compared with the original measured profiles, provide a check on the procedure and can be used to examine the validity of ignoring  $(1/r)(\partial V_r/\partial \theta)$  in deriving equation (20). The latter may be used to define those regions where the wandering contributions to the measured stresses are significant. As long as they are not overwhelming, wandering contributions may then be subtracted to obtain more credible turbulence distributions.

### 3.3. Implementation

Curve fits to measured vortex-core velocity profiles, using the series in equations (18) and (20), were performed by the method of least squares. This involved choosing in advance the number of terms in each series,  $n$  (typically 20 – about half the number of

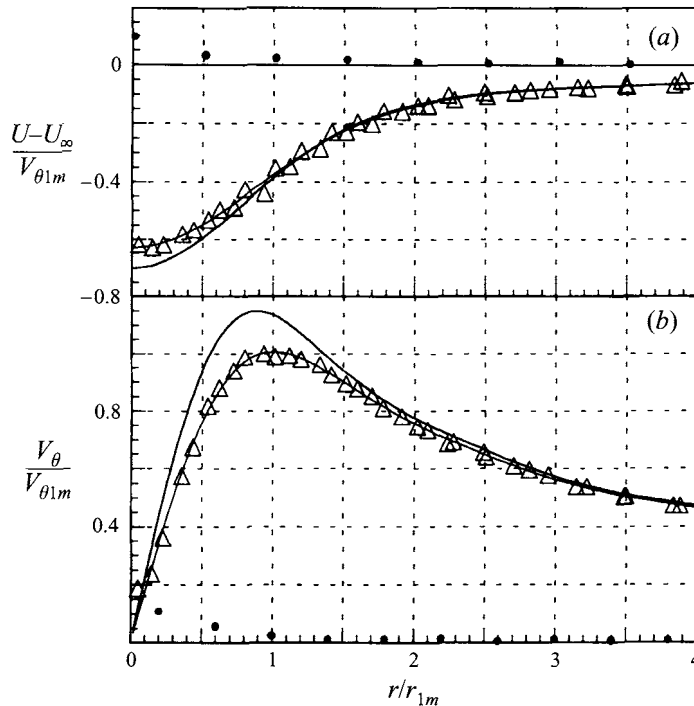


FIGURE 4. Comparison of (a) axial and (b) tangential velocity profiles at  $x/c = 30$  in the baseline flow. Triangles, measured velocity profiles; thin lines, curve fits to those profiles; thick lines, profiles corrected for wandering; dots, uncertainty due to correction procedure.

measured points), and the coefficients  $c_i$ . These coefficients define the radial scale of the function described by each term. Note that, for a given wandering amplitude, there is a minimum for  $c_i$  given by the solution to equation (19) for  $a_i^2 = 0$ , i.e.  $c_i > [2\sigma_z^2(1 - e^2)]^{1/2}$ . Physically this is the smallest radial scale that can result from wandering of the true profile. Beyond satisfying this requirement, values of  $c_i$  were chosen to be linearly spaced at about twice the measured point spacing.

As long as the  $c_i$  were fixed to give a wide range of radial scales, the resulting curve fits appeared very good in all cases (judged visually and by their r.m.s. error). The exact choice of the  $c_i$  had a greater influence on the profiles once they had been corrected for wandering, implying some uncertainty in the process. This uncertainty was estimated as twice the r.m.s. of variations in the corrected profile produced from a range of different initial curve-fit parameters. In many cases this turned out to be less than the measurement uncertainty in the original data. Uncertainty contributions associated with the correction process were greatest over the inner 40% or so of the core radius and increased with wandering amplitude. As an example, figure 4 shows axial and tangential velocity profiles through the present trailing vortex core at  $x/c = 30$  in the baseline flow (see table 2). This case was one of the most uncertain because wandering amplitudes were large ( $\sigma_y = 0.312r_{1m}$ ,  $\sigma_z = 0.285r_{1m}$ ,  $e = 0.266$ ) and scatter in the raw measurements was greatest. Included in figure 4 are the measured points, the curve fits through those points, those curve fits corrected for wandering and estimates of uncertainty introduced by the corrections. Despite the scatter the curves accurately described the form of the measured profiles. Uncertainties introduced by the correction process are small except close to the core centre, but even there are less than 15%  $V_{\theta 1m}$ . The corrected profiles show a 12% smaller core radius, 15% greater tangential velocity

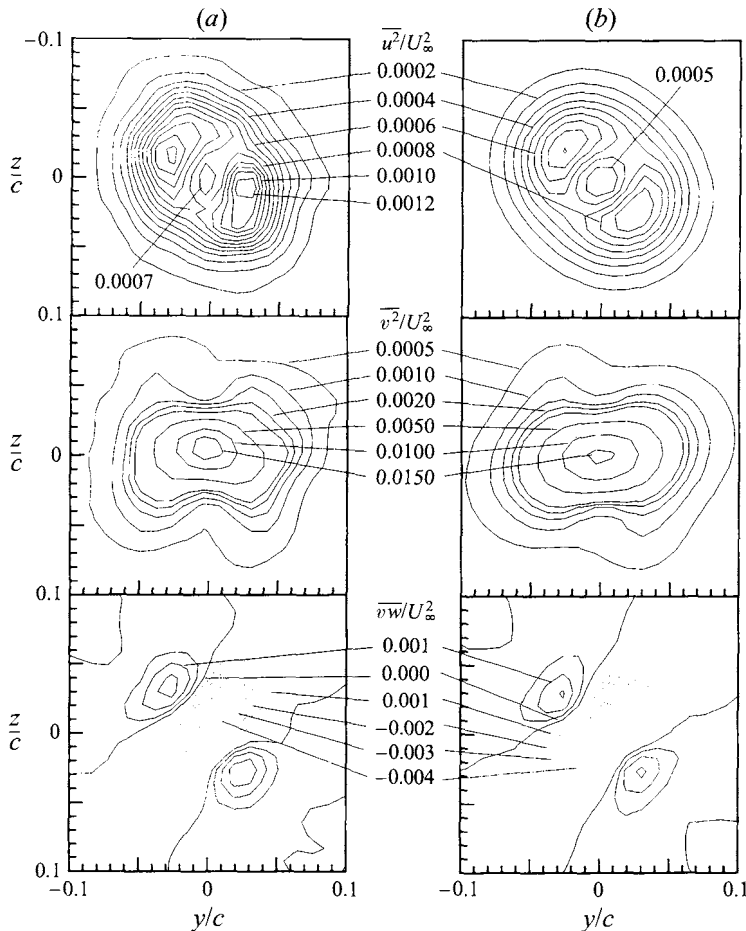


FIGURE 5. Comparison of Reynolds stress: (a) measurements and (b) computed from estimated wandering amplitudes and corrected mean-velocity fields. Baseline flow,  $x/c = 30$ . Note measured core diameter  $= 0.082c$ . Measured and computed data represented using same absolute contour levels.

and an 11% greater axial velocity deficit than those originally measured. These lie fairly close to the values of 12%, 14% and 8% predicted by the 'rules of thumb' in equations (9), (10) and (12) with  $\sigma = [\frac{1}{3}(\sigma_y^2 + \sigma_z^2)]^{1/2}$ .

One way of checking the corrected profiles and the wandering amplitudes is to use equation (4) to compute the apparent stress fields that they imply. Detailed measurements of stress fields in the vicinity of the core were taken to compare with these predictions. The comparison (figure 5) shows surprisingly good agreement between measured and computed contours of  $\overline{v^2}$  and  $\overline{vw}$ , suggesting that these are dominated by wandering. Similar agreement is seen in comparisons of  $\overline{w^2}$ ,  $\overline{uw}$  and  $\overline{uw}$  (not shown). The measurements of  $\overline{u^2}$  agree less well, lying about 30% above the computed values. Presumably this is because the wandering contributions to  $\overline{u^2}$  are more than an order of magnitude smaller than those to other normal stresses, making it probable that other sources of velocity fluctuations are significant.

The close agreement between measured and predicted stress fields is encouraging and suggests that the corrected velocity fields and the inferred wandering amplitudes may be accurate. The accuracy of the predictions appears at least sufficient to define regions

where wandering contributions to the measured stresses are significant. An inadvertent byproduct of the comparisons in figure 5 is that they demonstrate a certain level of accuracy in the hot-wire Reynolds stress measurements. It also seems very unlikely that such accuracy could be achieved in the core region if probe interference were a significant factor.

#### 4. Results and discussion

Experiments were performed over the range of conditions listed in table 2. Most measurements were made to document the development and structure of the baseline flow, generated at a chord Reynolds number  $U_\infty c/\nu$  of 530 000 with the wing at an angle of attack  $\alpha$  of  $5^\circ$  and with the 20%–40% trip attached. Grids of velocity measurements were made at cross-sections  $5c$ ,  $10c$ ,  $15c$ ,  $20c$ ,  $25c$  and  $30c$  downstream of the wing leading edge to reveal the roll-up of the vortex and the turbulence structure and scaling outside the core region. Detailed velocity profiles and fine grids were also measured at these stations to reveal the mean flow and turbulence structure in the core region. To determine the scaling of velocity fluctuations in the core region, velocity profiles were also measured in other flows generated with the wing at different angles of attack (to vary core strength), with different trips (to vary wake strength) and at different Reynolds numbers. Table 2 lists vortex core parameters measured at all these conditions and locations. Table 3 lists typical uncertainties in velocity measurements.

The rectangular and cylindrical coordinate systems illustrated in figure 1 will be used in presenting measurements. Distance  $x$  is measured downstream from the wing leading edge. Distances  $y$ ,  $z$  and  $r$  are measured from the vortex centre, unless otherwise stated. Velocity components  $U$ ,  $V$  and  $W$  are defined in the directions of  $x$ ,  $y$  and  $z$  respectively.

Small-amplitude vortex wandering motions were present to a varying extent at all conditions and locations. During measurements in the core, the wandering was visible as a low-frequency fluctuation in the velocity signal.  $V$  and  $W$  velocity fluctuations at the core centre were in all cases dominated by this fluctuation, spectral measurements showing typically 95% of the energy in these signals lying at frequencies below  $fc/U_\infty = 1$ . Anisotropy of the wandering motions was first indicated by velocity fluctuation measurements at the core centre which in all cases showed unequal  $\overline{v^2}$  and  $\overline{w^2}$  and non-zero  $\overline{vw}$  (see figure 5a for example). This anisotropy is a consequence only of the very slowest motions –  $V$  and  $W$  autospectra measured at the core centre differing only for frequencies below  $fc/U_\infty = 0.01$  ( $= 2$  Hz for  $U_\infty = 40$  m s $^{-1}$ ), see Devenport *et al.* (1992). Long averaging times (typically 120 s) were necessary to obtain statistically stationary results in the presence of these motions.

Amplitudes of wandering, determined from core velocity profiles using the method described in §3.2 (see table 2), were in all cases a fraction of the core radius. Figure 6 shows the amplitudes as functions of streamwise position in the baseline flow and as functions of angle of attack at a fixed position. The wandering amplitudes increase roughly linearly with downstream distance and decrease with the angle of attack of the wing. The latter variation suggests that the most important source of the wandering may have been wind-tunnel unsteadiness, since this would decrease in importance as the strength of the vortex was increased. (Test-section flow-direction changes of only  $0.025^\circ$  r.m.s. would be enough to account for the wandering motions in the baseline flow.) This conjecture would seem to be supported by the fact that the preferred direction of wandering was almost the same in every case – between  $53^\circ$  and  $69^\circ$  from the  $z$ -axis toward the  $y$ -axis (see table 2). It is also consistent with the inferences of



Case	Conditions			Vortex core parameters							Wandering		Angle† (deg.)
	$U_\infty c/\nu$	$\alpha$ (deg.)	$x/c$	Trip (%)	$r_1/c$	$V_{\theta 1}/U_\infty$	$U_D/U_\infty$	$\Gamma_1/\Gamma_0$	$\Gamma_1/\nu$	$U_D/V_{\theta 1}$	$\sigma_y/c$	$\sigma_z/c$	
1	530000	5	5	20-40	0.036	0.286	0.165	0.267	33900	0.577	0.004	0.004	56.6
2	530000	5	10	20-40	0.037	0.286	0.152	0.275	35000	0.531	0.007	0.005	68.5
3	530000	5	15	20-40	0.036	0.277	0.141	0.261	33200	0.511	0.008	0.006	59.9
4	530000	5	20	20-40	0.039	0.278	0.153	0.287	36500	0.55	0.009	0.007	56.9
5	530000	5	25	20-40	0.033	0.275	0.147	0.236	30000	0.534	0.01	0.009	53.6
6	530000	5	30	20-40	0.036	0.263	0.16	0.248	31600	0.609	0.013	0.012	54.6
7	400000	5	30	20-40	0.039	0.285	0.172	0.289	27700	0.603	0.012	0.011	57.0
8	260000	5	30	20-40	0.044	0.295	0.169	0.337	21000	0.575	0.01	0.008	68.6
9	530000	7.5	10	20-40	0.045	0.422	0.085	0.329	62700	0.202	0.006	0.005	63.1
10	530000	3.75	10	20-40	0.021	0.231	0.16	0.167	15900	0.693	0.006	0.006	59.1
11	530000	2.5	10	20-40	0.019	0.166	0.144	0.164	10400	0.867	0.009	0.008	53.2
12	530000	5	10	None	0.038	0.291	0.086	0.29	36900	0.297	0.006	0.004	68.7
13	530000	5	10	0-40	0.033	0.263	0.181	0.225	28700	0.686	0.008	0.007	61.7
14*	530000	5	10	20-40	0.027	0.34	0.195	0.239	30500	0.574	0.006	0.005	63.1

\* Wing tip rounded using half-body of revolution.

† Angle of principle axis of wandering measured from the z-axis toward the y-axis.

TABLE 2. Flow conditions, vortex core parameters and characteristics of the wandering motions for all measurement cases. Note that cases 1-6 are in the baseline flow and that core parameters are deduced from mean-velocity profiles corrected for wandering using the method of §3.2

\* Wing tip rounded using half-body of revolution.

† Angle of principle axis of wandering measured from the  $z$ -axis toward the  $y$ -axis.

TABLE 2. Flow conditions, vortex core parameters and characteristics of the wandering motions for all measurement cases. Note that cases 1–6 are in the baseline flow and that core parameters are deduced from mean-velocity profiles corrected for wandering using the method of §3.2

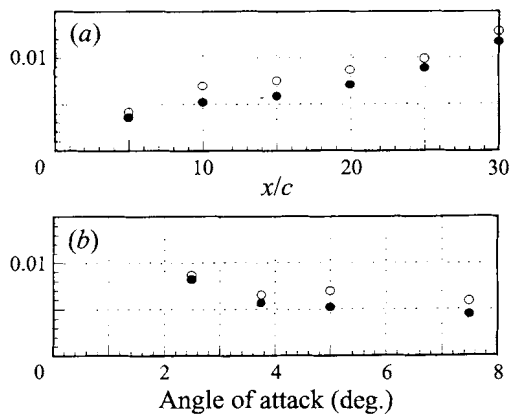


FIGURE 6. Wandering amplitudes (a) in the baseline flow and (b) as a function of angle of attack at  $x/c = 10$ . Open circles;  $\sigma_y/c$ , filled circles;  $\sigma_z/c$ .

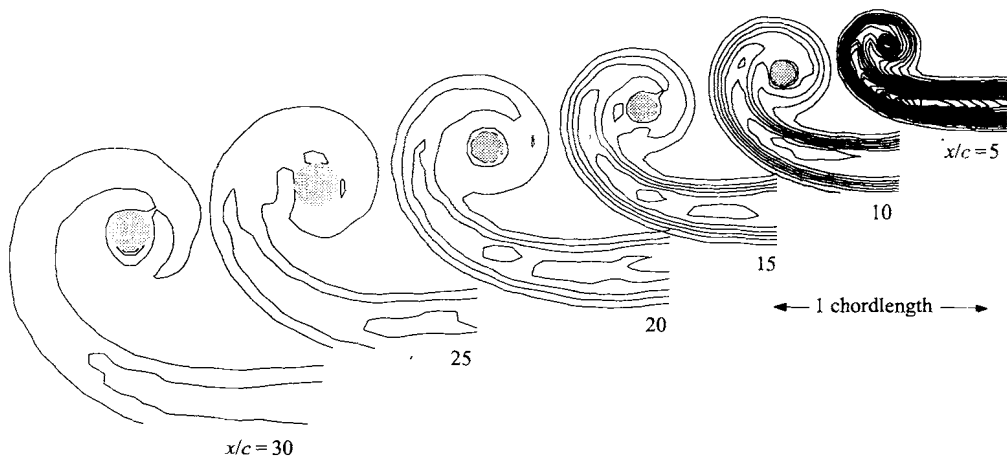


FIGURE 7. Contours of axial normal turbulence stress in the baseline flow normalized on  $U_\infty$ . Contours are at intervals of  $5 \times 10^{-5}$ . Shaded regions are where the contribution from wandering exceeds 30% of measured stress.

Quantity	Uncertainty	
	Spiral wake	Core
$U, V, W$	0.015	0.015
$\frac{\omega_x}{u^2}$	0.034	—
$\frac{v^2}{u^2}$	$3.1 \times 10^{-6}$	$1.4 \times 10^{-5}$
$\frac{w^2}{u^2}$	$9.5 \times 10^{-6}$	$1.5 \times 10^{-5}$
$\frac{\overline{uv}}{u^2}$	$9.9 \times 10^{-6}$	$2.0 \times 10^{-5}$
$\frac{\overline{vw}}{u^2}$	$4.3 \times 10^{-6}$	$1.4 \times 10^{-5}$
$\frac{\overline{uw}}{u^2}$	$4.5 \times 10^{-6}$	$2.3 \times 10^{-5}$
$\frac{\overline{uv}}{u^2}$	$2.9 \times 10^{-6}$	$8.5 \times 10^{-6}$

TABLE 3. Uncertainties in velocity measurements calculated for 20:1 odds at typical locations in spiral wake and core regions. All uncertainties are in terms of  $U_\infty$ ,  $U_\infty/c$  or  $U_\infty^2$  as appropriate

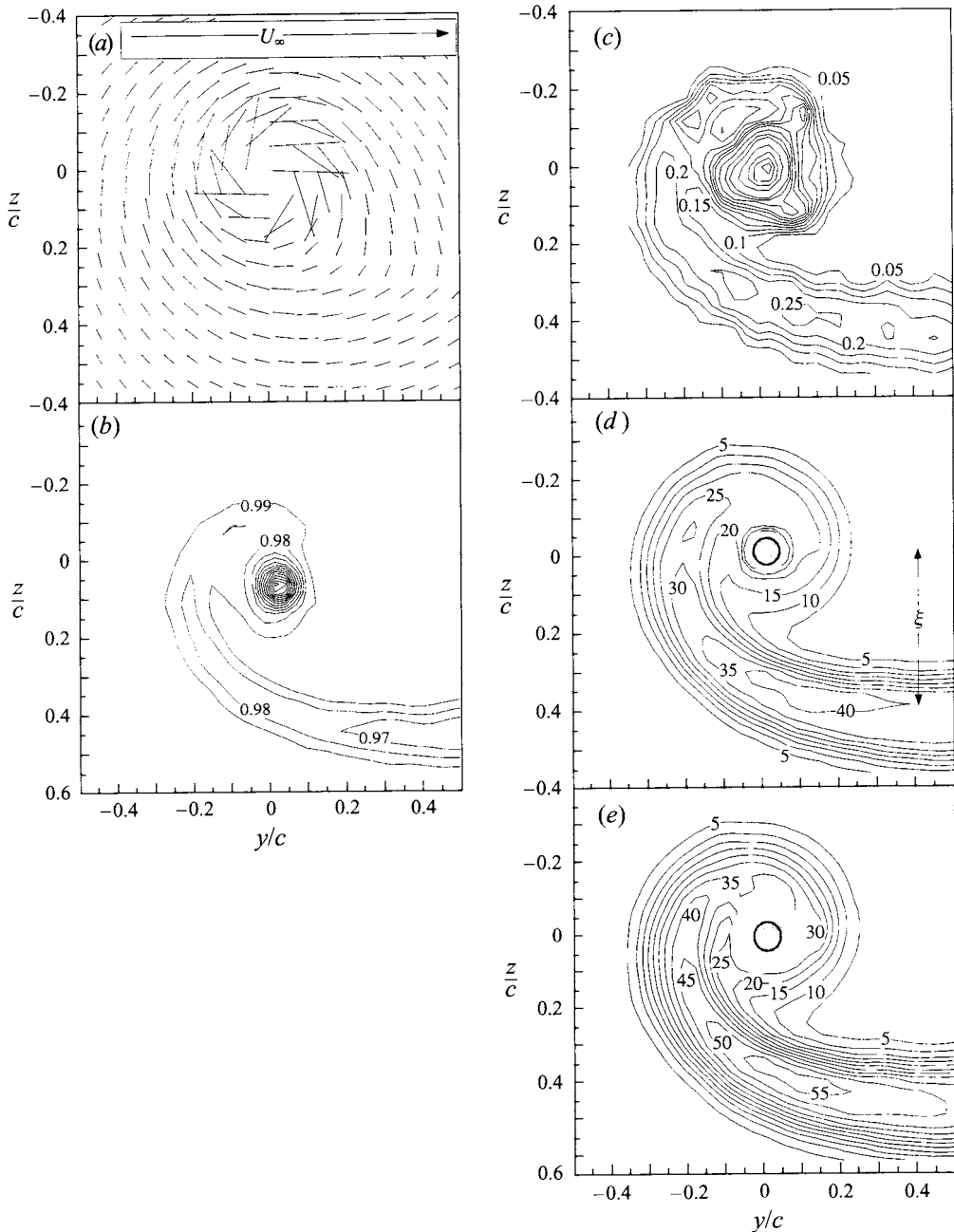


FIGURE 8. Velocity measurements at  $x/c = 10$  in the baseline flow. (a) Mean cross-flow velocity vectors. (b) Contours of  $U/U_\infty$ . (c) Mean streamwise vorticity  $\omega_x c/U_\infty$  obtained by differentiating grid data. (d) Axial normal stress  $u^2/U_\infty^2 \times 10^5$ . (e) Turbulence kinetic energy  $k/U_\infty^2 \times 10^5$ . Shading covers regions where wandering contributions were  $> 30\%$ . Solid line shows core edge. Note that contours are not accurate in the vicinity of the core due to the large grid spacing.

previous authors, most notably Baker *et al.* (1974) and Reed (1973). Wandering amplitudes were used to correct mean velocity profiles and estimate the contributions of wandering to turbulence stress fields. Corrections and contributions were negligible outside the core regions (typically  $r/c > 0.1$ ).

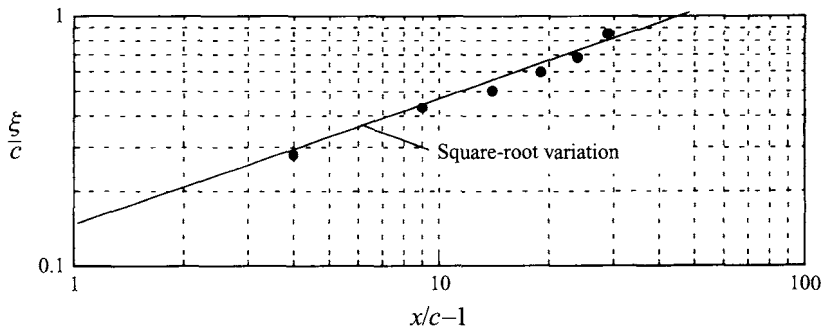


FIGURE 9. Scale of the wake spiral  $\xi$  (see figure 8*d*) as a function of  $x/c$  in the baseline flow.

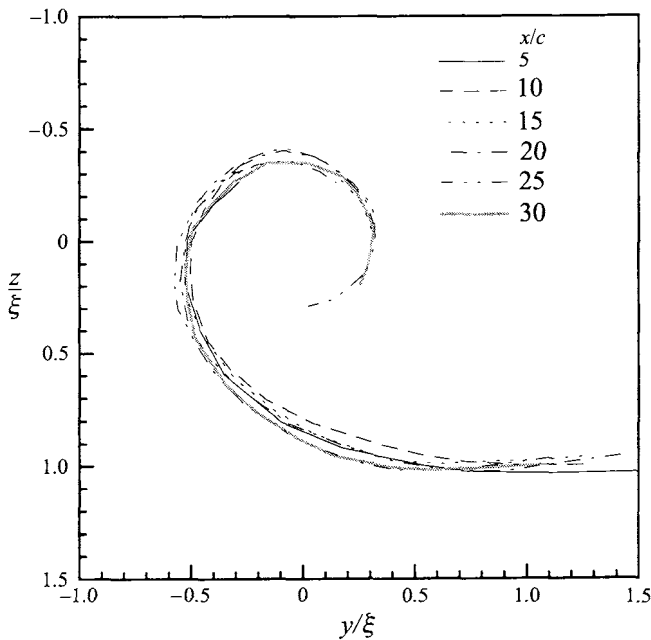


FIGURE 10. Shape of the wake spiral (defined as the locus of peak axial normal turbulence stress) normalized on  $\xi$  as a function of  $x/c$  in the baseline flow.

4.1. Overall form of the vortex

Figure 7 illustrates the overall form of the vortex in the baseline flow in terms of contours of axial normal turbulence stress  $\overline{u^2}/U_\infty^2$ . More detailed views of the flow structure outside the core region are given for  $x/c = 10$  by the mean cross-flow velocity vectors and contours of  $U/U_\infty$ , mean streamwise vorticity  $\omega_x c/U_\infty$ ,  $\overline{u^2}/U_\infty^2$ , and turbulence kinetic energy  $k/U_\infty^2$  shown in figure 8.

The flow consists of a small concentrated vortex core (of radius between  $0.03c$  and  $0.04c$ , table 2) surrounded by a circulating velocity field (figure 8*a*) that winds the rest of the wing wake into an ever-increasing spiral. The scale of the spiral  $\xi$ , measured as the  $z$  distance between the vortex centre and lowest point of the wake centreline (defined by the locus of peak  $\overline{u^2}/U_\infty^2$ ), see figure 8(*d*), grows approximately as the square root of  $x$  (figure 9). Interestingly, the shape of the spiral centreline is roughly self-similar when normalized on  $\xi$  (figure 10). The mean vorticity contours of figure

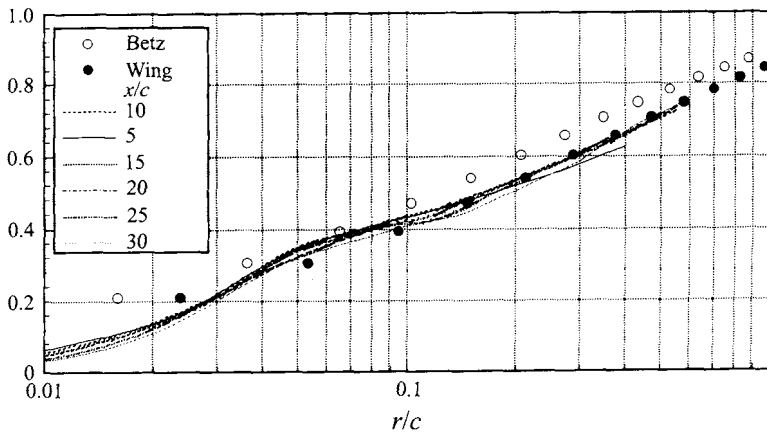


FIGURE 11. Circulation profiles in the baseline flow compared with lifting-line theory and Betz's theory predictions.

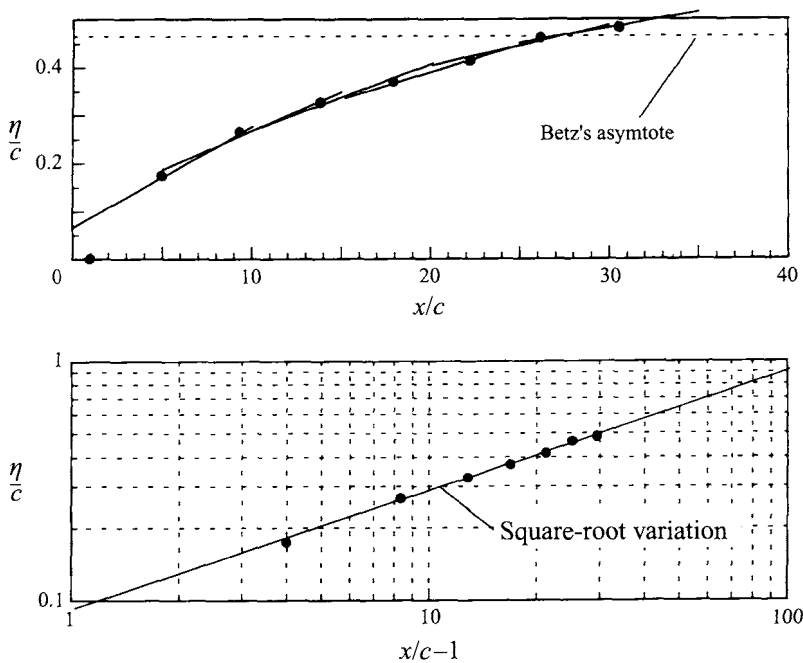


FIGURE 12. Spanwise position of the core  $\eta$  as a function of  $x/c$  in the baseline flow. Points deduced from flow visualization. Tangents in upper figure show direction of core deduced from hot-wire measurements.

8(c) and circulation distributions of figure 11 show the wake spiral to contain a substantial proportion of the streamwise vorticity shed by the wing. The circulation distributions, computed by integrating the profile and gird data on circular paths, are compared with predictions of the circulation distribution on the wing (from lifting-line theory) and in the vortex. The latter was obtained from the theoretical wing circulation distribution using Betz's (1933) theory (as simplified by Rossow 1973 and Donaldson, Snedeker & Sullivan 1974), which assumes inviscid two-dimensional flow, axisymmetry and complete roll-up of the vortex. All curves are normalized on the theoretical root circulation  $\Gamma_0$ .  $\Gamma/\Gamma_0$  increases monotonically with radius at all stations indicating that

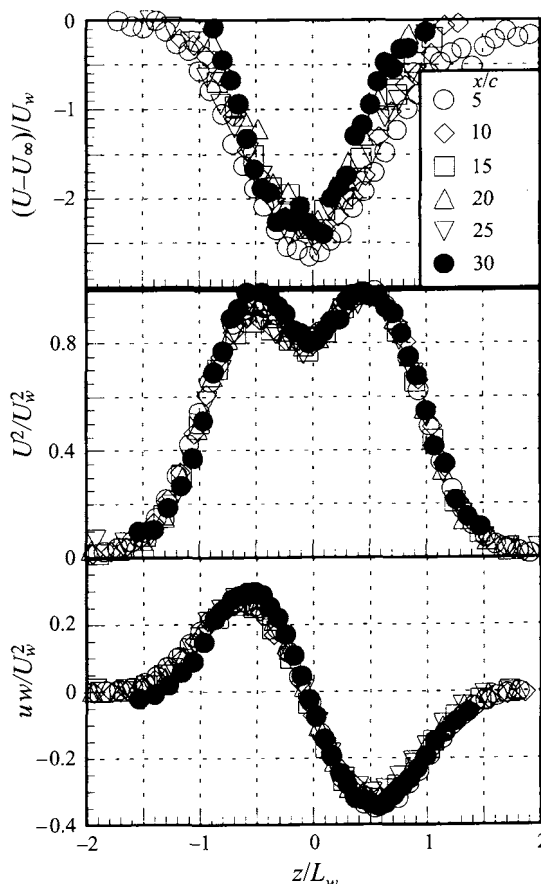


FIGURE 13. Velocity profiles measured through the wake at  $y/c = 2.5$  (measured relative to the wing-tip location) normalized on scales  $U_w$  and  $L_w$  defined in terms of the  $u^2$  profile the  $z$  origin is at the wake centreline.

the vortex is stable according to Rayleigh's criterion. Outside the core region ( $r/c > 0.1$ ) the circulation distribution lies closest to the lifting-line theory prediction and varies little with distance downstream. Closer to the core, where the wake spiral is well merged and the flow more axisymmetric (i.e. near  $r/c = 0.05$ ), there is initially some agreement with Betz's theory. However, this disappears at around  $x/c = 20$  where the circulation at this radius begins to fall, perhaps indicating some outward diffusion of vorticity associated with the thickening of the wake spiral.

The trajectory of the vortex core is shown in figure 12 in terms of distance  $\eta$ , defined as the  $y$ -coordinate of the vortex core centre relative to the wing tip. This trajectory was deduced from helium-bubble flow visualizations performed at a lower Reynolds number (130 000) but is closely consistent with angles between the core and free-stream flow direction inferred from the hot-wire measurements. As one would expect, the core is seen to move inboard at a rate that decreases with distance downstream. Plotted on logarithmic scales,  $\eta$  (like  $\xi$ ) is seen to vary as the square root of streamwise distance. Figure 12 also shows an estimate of the centroid of the vorticity distribution shed from the wing obtained using lifting-line theory. According to Betz's theory the vortex centre should asymptote to this position. In reality the path of the vortex crosses this asymptote at about  $x/c = 26$ , apparently moving toward a location further inboard.



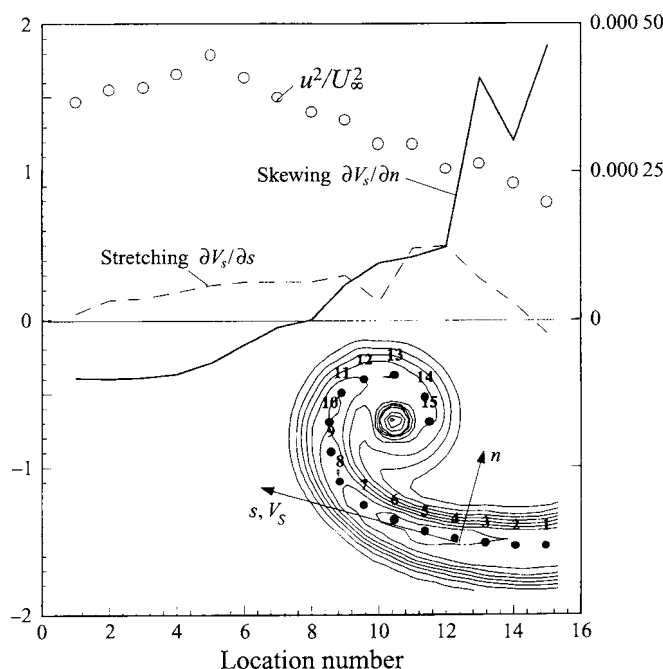


FIGURE 14. Rates of strain and turbulence stress on the spiral wake centreline at  $x/c = 10$  in the baseline flow. Strain rates normalized on the maximum axial velocity gradient in the two-dimensional portion of the wake. Locations and symbols defined in the lower part of figure.

#### 4.2. Turbulence structure and scaling outside the core region

Figure 8(d, e) shows the turbulence structure outside the core region at  $x/c = 10$  in detail. This is dominated by the wake spiral, any region of axisymmetric turbulent flow around the core being small, if present at all. Turbulence levels vary along the spiral. Far from the core, in the flat part of the wake, the structure of the flow appears much like that of a two-dimensional turbulent wake. Mean axial velocity and Reynolds stress profiles (figure 13) and velocity autospectra measured here are similar to those presented by Wygnanski, Champagne & Marasli (1986) and Antonia & Britz (1989). Three-dimensional effects become apparent as one moves outboard. Peak turbulence levels first rise, reaching a maximum at  $y/c = 0.1$ ,  $z/c = 0.38$  near where the wake begins to curve. They then fall monotonically as the core is approached along the spiral.

These variations are presumably a consequence of the mean rates of strain and lateral curvature suffered by the turbulence. Figure 14 shows mean rates of stretching and skewing at the spiral wake centreline (determined by differentiating the grid measurements) normalized upon  $S_{2D}$ , the peak mean axial velocity gradient  $\partial U/\partial z$  in the two-dimensional part of the wake. Also plotted in figure 14 is the peak axial turbulence stress. Far from the core the rate of skewing is small and negative at about  $-0.4S_{2D}$  but then increases rapidly, passing through zero at location 8 (near the maximum in  $\bar{u}^2$ ) and then through 1.0 at location 13. The magnitude of the stretching is smaller at most locations and remains approximately constant at about  $0.25S_{2D}$ . Positive skewing and stretching are generated by the rotational velocity field of the vortex, specifically  $\partial V_\theta/\partial r$ . Negative skewing is associated with the streamwise vorticity embedded within the wake itself (figure 8c).

The additional rates of strain appear to influence turbulence levels by inhibiting the

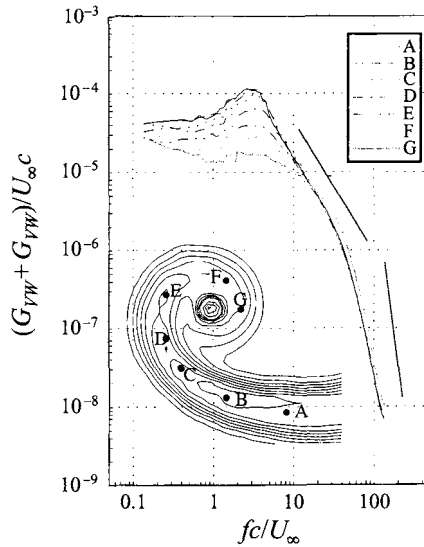


FIGURE 15. Velocity autospectra at selected locations along the spiral-wake centreline at  $x/c = 10$  in the baseline flow.

larger turbulent eddies. Velocity autospectra  $G_{UU}$  and  $G_{VV} + G_{WW}$  (we plot the sum of  $V$  and  $W$  autospectra since this is invariant to rotation in the cross-flow plane), measured at points along the wake centreline (figure 15 for example), show a substantial drop in low-frequency energy as the rates of strain increase. The drop is greatest around the peak in  $G_{VV} + G_{WW}$  near  $fc/U_\infty = 3$  which, following the work of Antonia & Britz (1989) and others, we would expect to be associated with the dominant large-scale eddies. Interestingly, the suppression of these eddies has less effect on the smaller turbulence structures, at least as they are represented in the velocity spectrum. Spectral levels at frequencies above  $fc/U_\infty = 20$  remain at almost the same absolute values along the outer part of the spiral (locations A to E). Closer to the core they rise slightly (locations F and G) perhaps because of additional small-scale turbulence released by the breakup of large eddies in the very high strain rates here.

The streamwise development of turbulence structure outside the core is visible in figure 7. There is little sign of turbulence being sustained or generated by the rotational motion of the vortex outside the core region. Most of what is seen appears to be the decay of turbulence associated with the axial velocity deficit of the spiral wake. In the flat part of the wake far from the core the decay is like that of a self-similar two-dimensional wake. The evolution of velocity and turbulence profiles here (figure 13) can be described by a single length scale  $L_w$  and velocity scale  $U_w$  (defined here using the axial normal stress profile) which grow and decay approximately as the square-root of streamwise distance. Closer to the core the decay is accelerated by the additional rates of strain. Figure 16(a) shows the peak axial turbulence stress in the wake spiral (normalized on its value in the two-dimensional region  $U_w^2$ ) plotted as a function of radius for the six streamwise stations. At all radii less than  $0.5c$  the decay rate is significantly more rapid than in the two-dimensional region.

Interestingly, the data in figure 16(a) may be collapsed to a single curve if the radius is normalized on  $\xi$ , the scale of the spiral (figure 16b). This appears to be the result of an approximate self-similarity of the turbulence structure, which arises because of two coincidences. First, the scale of the spiral  $\xi$  and the wake thickness  $L_w$  both increase roughly as the square-root of  $x$ . This means that since the shape of the spiral centreline

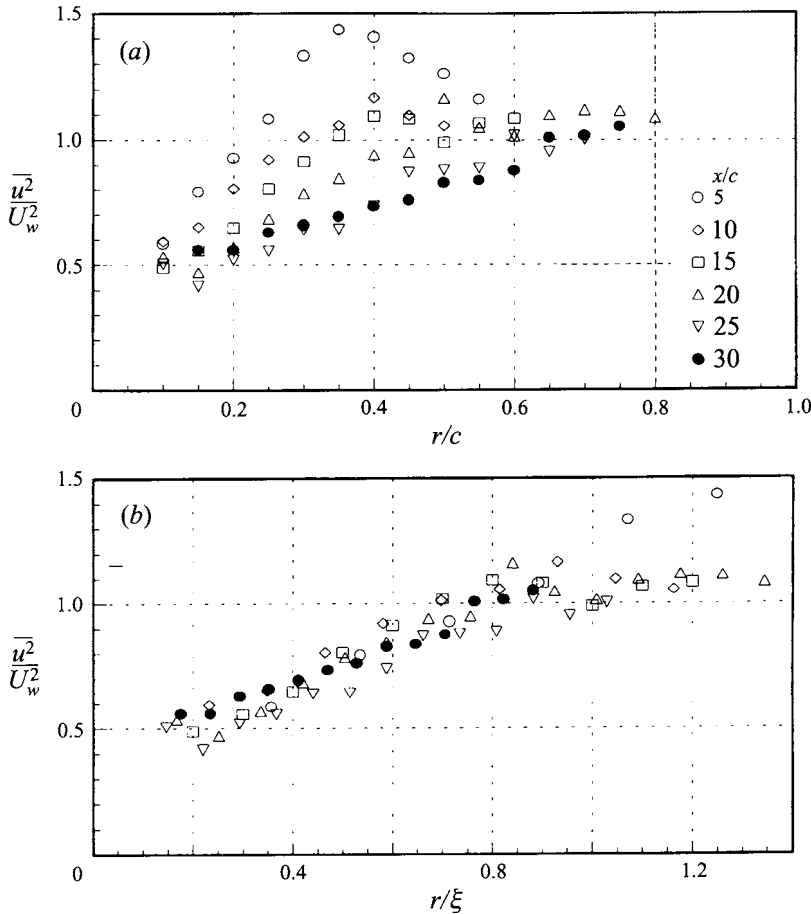


FIGURE 16. Peak axial normal turbulence stress in the wake spiral as a function of radius normalized on (a) chordlength, and (b) scale of the spiral. Baseline flow.

becomes constant when scaled on  $\xi$  (figure 10), so does the entire footprint of the wake. Secondly, the rates of strain  $S$  imposed by the tangential velocity field of the vortex upon the spiral wake vary as  $1/r^2$  at large radius since the circulation here varies only slowly. This makes them only a function of  $r/\xi$  when normalized on  $U_w$  and  $L_w$ , i.e.

$$\frac{SL_w}{U_w} \sim \frac{L_w}{r^2 U_w} = \frac{\xi^2}{r^2} \frac{L_w}{\xi^2 U_w} \sim \frac{\xi^2}{r^2},$$

which follows given the square-root variations in  $\xi$ ,  $L_w$  and  $U_w$ .

Approximate self-similarity in the footprint of the spiral wake and in the rate of strain it experiences when scaled on  $U_w$  and  $\xi$  leads to the self-similarity of the turbulence stress field that was hinted at in figure 16(b). The extent of this self-similarity may be illustrated by re-plotting the turbulence stress contours of figure 7 scaled on  $U_w$  and  $\xi$ , as is done in figure 17. In these terms, there is little variation in the turbulence structure downstream of  $x/c = 10$ .

It is worth noting that self-similarity of the turbulence stress field is not a forgone conclusion given similarity of the rates of strain. The above analysis implies that a fixed radius and thus, presumably, a given body of wake turbulence, experiences a non-dimensional rate of strain that increases linearly with  $x$ . History effects in the

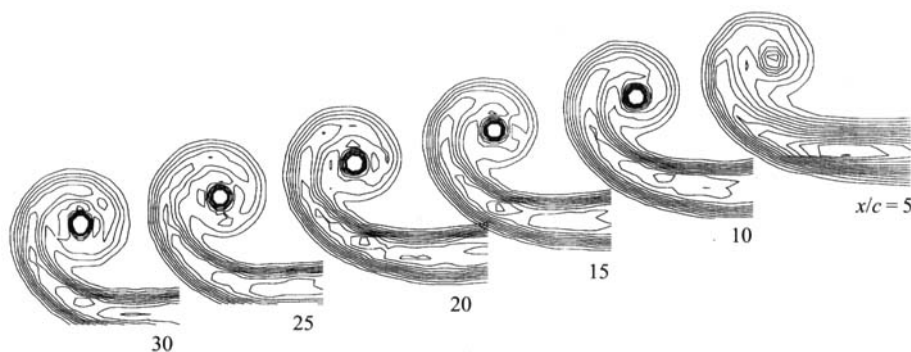


FIGURE 17. Axial normal stress data of figure 7 normalized on similarity variables  $U_w$  and  $\xi$ . Contours at intervals of 0.1.

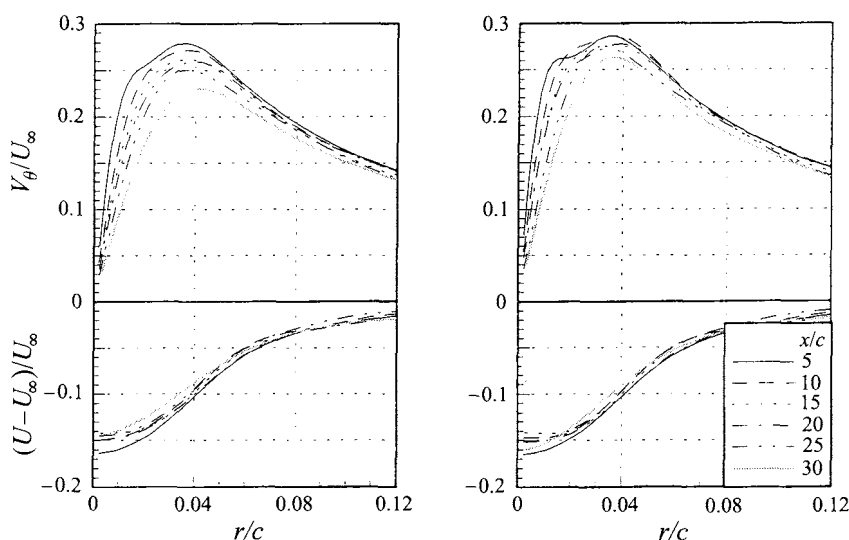


FIGURE 18. Mean tangential and axial velocity profiles through the core in the baseline case (a) uncorrected and (b) corrected for the effects of wandering.

turbulence would therefore work against self-similarity. However, the increase is slow (a factor of 3 from  $x/c = 10$  to 30 – a distance equivalent to over 200 initial  $L_w$  values) and thus the turbulence may have time to adjust.

#### 4.3. Mean flow structure in the core region

Figure 18 shows mean axial  $U$  and tangential  $V_\theta$  velocity profiles through the core region in the baseline flow at the six  $x$  stations. All profiles were measured parallel to the  $z$ -axis. The radial velocity component is not plotted since in the core region it was zero to within the measurement uncertainty. To obtain these profiles it was necessary to resolve the velocity components in core-aligned coordinates (to compensate for the small angle between the core centreline and free stream, see figure 12) and then identify the core centre as the point of zero cross-flow velocity.

Figure 18 shows the profiles both before and after correcting for the smoothing effects of wandering using the method of §3.2. The uncorrected profiles show apparent growth of the core, decay of the peak tangential velocity, decay of the axial velocity deficit and some changes in the shape of the tangential profiles. Correcting for

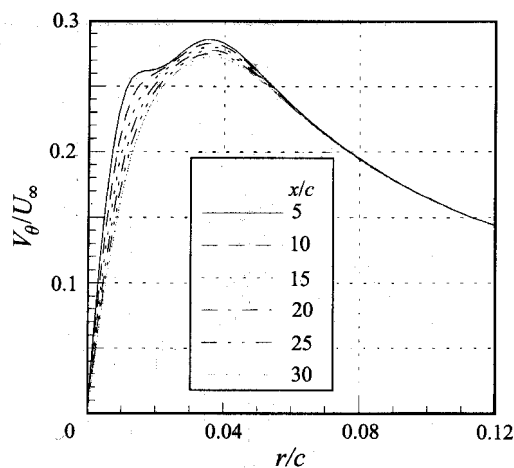


FIGURE 19. Development of tangential velocity profiles in the baseline flow computed assuming laminar flow starting with the measured profile at  $x/c = 5$ .

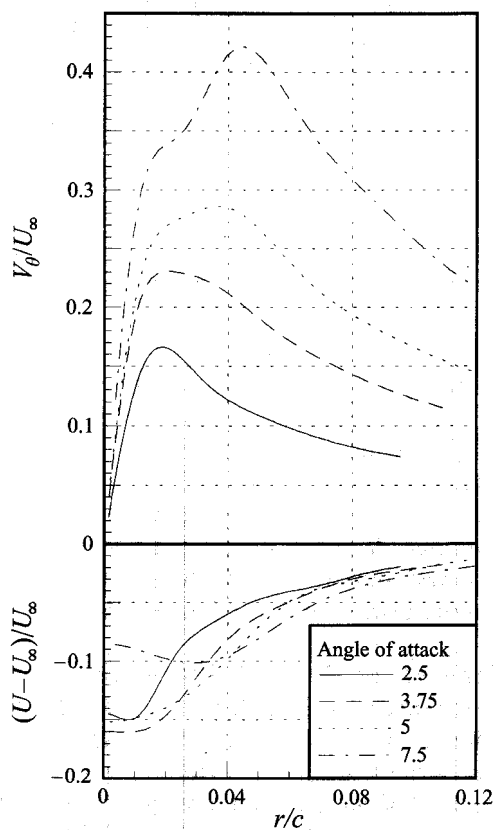


FIGURE 20. Mean tangential and axial velocity profiles through the core at  $x/c = 10$  as functions of angle of attack. Profiles corrected for the effects of wandering.

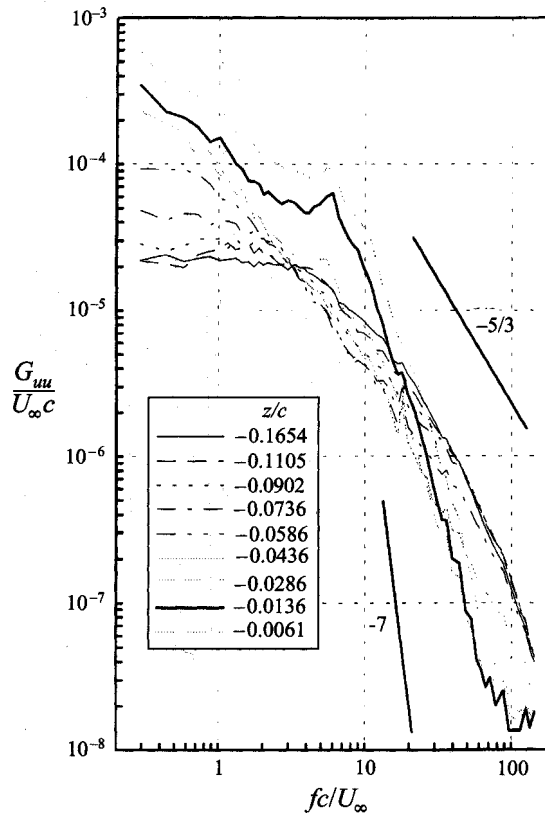


FIGURE 21.  $U$ -component autospectra along a  $z$ -wise profile from the spiral wake to the core centre in the baseline flow at  $x/c = 10$ .

wandering reduces the apparent growth and decay of core parameters, but accentuates some of the changes in profile shape. In the corrected profiles the peak tangential velocity, core radius and axial velocity deficit remain constant to within the measurement uncertainty at about  $0.27U_\infty$ ,  $0.036c$  and  $0.155U_\infty$  respectively. These imply a core circulation  $\Gamma_1$  of 26% of  $\Gamma_0$ , a core circulation Reynolds number  $\Gamma_1/\nu$  of 33000 and a Rossby number  $Ro$  (axial deficit over peak tangential velocity) of 0.57. The changes in profile shape include a factor of two to three decay in the tangential velocity gradient at the core centre, and the disappearance of an inflection seen in the  $V_\theta$  profile at  $x/c = 5$ .

Much of the development of the tangential velocity field seen in figure 18 is sufficiently slow to be accounted for entirely by viscous diffusion. Figure 19 shows the development of the tangential profile computed assuming laminar, cylindrical flow ( $v_r = 0, u \neq f(x)$ ) starting with the measured profile at  $x/c = 5$ . Between  $x/c = 5$  and 20 the measured and computed development are very similar. Between  $x/c = 20$  and 30 the measured decay appears faster, but this may well be due to greater uncertainty associated with the wandering corrections at  $x/c = 25$  and 30.

The inflection point seen in the profile at  $x/c = 5$  and the manner of its disappearance suggest a two layered structure – an inner core that grows with downstream distance and an outer core of approximately constant radius. Evidence for such a structure is also seen in some of the other flows. Figure 20 shows corrected tangential and axial velocity profiles measured at  $x/c = 10$  as a function of wing angle of attack. At  $2.5^\circ$



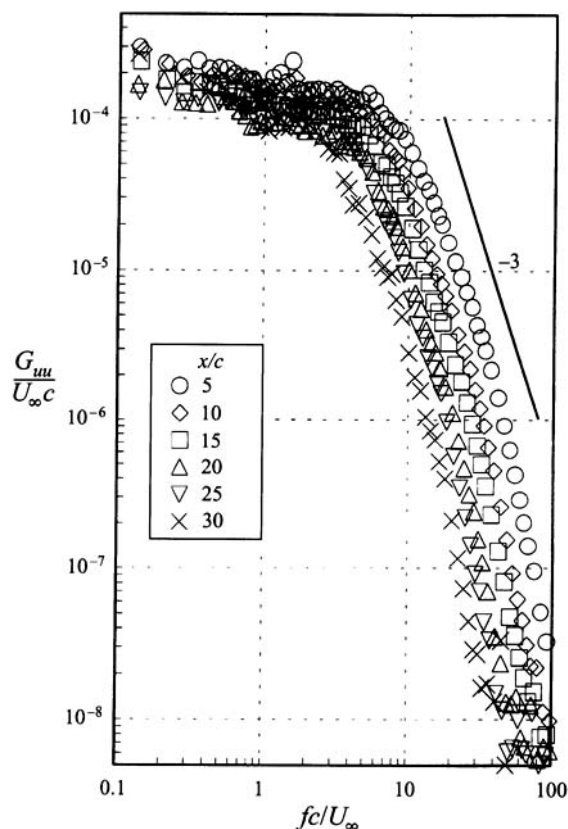


FIGURE 22.  $U$ -spectra at the core centre in the baseline flow normalized on free-stream velocity and chordlength.

only a single core edge is seen at a radius of about  $0.02c$ . The other profiles, however, show evidence for two core edges, one apparently fixed near  $r/c = 0.02$ , and the other increasing in radius with angle of attack from  $0.03c$  at  $3.75^\circ$  to  $0.045c$  at  $7.5^\circ$ . There is even some evidence of a double core in the axial profile at  $7.5^\circ$ , which appears to show a small axial velocity surplus superimposed upon a larger deficit. Note that none of these features are pure products of the wandering corrections. All are seen in the uncorrected data.

It seems likely that the double core is a remnant of the initial condition. Helium-bubble flow visualizations of the flow around the present wing tip (Engel 1995) show not only the formation of the main tip vortex, first visible at about mid-chord on the suction side, but also the roll-up of a strong corotating secondary vortex from the pressure side of the tip. For about one chordlength downstream of the trailing edge these vortices rotate about each other but the secondary vortex soon becomes invisible. At the same time the spiral motion of the main tip vortex associated with the interaction also dies out. Given the results of Corsiglia, Iversen & Clifone (1976), Steger & Cutler (1976), Brandt & Iversen (1977) and Bilanin, Teske & Williamson (1977), all of whom studied the interaction of unequal corotating vortices, we would expect the vorticity associated with the secondary vortex to have become wrapped into an annulus around the main vortex core. This would likely produce the double core structure we have observed.

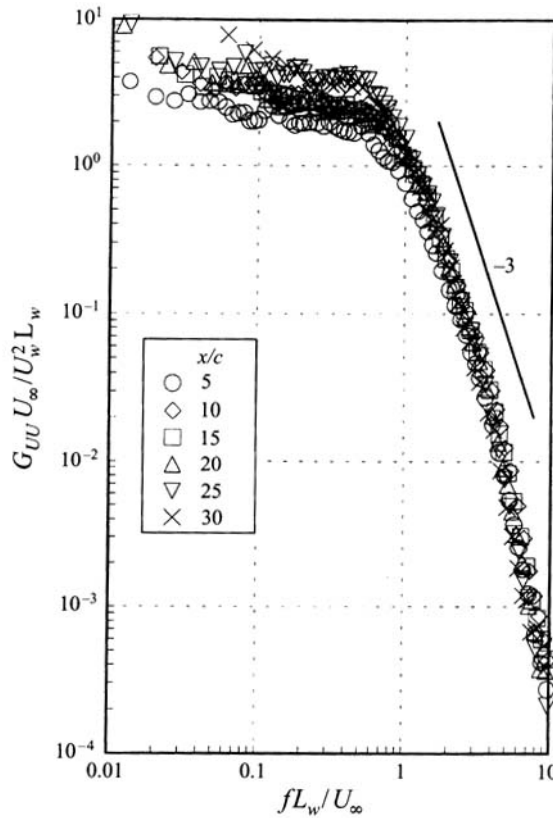


FIGURE 23.  $U$ -spectra at the core centre in the baseline flow normalized on two-dimensional wake parameters.

#### 4.4. Turbulence structure and scaling in the core region

To reveal the turbulence structure of the core region it was necessary to separate out those velocity fluctuations generated by wandering. This was done by spectral decomposition and high-pass filtering.

##### 4.4.1. Spectral decomposition

Some clues to the true turbulence structure in the core region are given by the series of velocity autospectra shown in figure 21. These were measured in the baseline flow at  $x/c = 10$  along the line  $y/c = 0$  from the spiral wake centreline at  $z/c = -0.1654$  to the core centre (see figure 8*d*). At frequencies less than  $fc/U_\infty = 20$ , spectral levels rise as the core centre is approached because of wandering and, as we shall see, other inactive motions of the core. At frequencies greater than  $fc/U_\infty = 20$ , where we would expect to see the influence of smaller turbulent structures, spectral levels fall, becoming an order of magnitude smaller at the core centre than they are in the wake. Even in the region just outside the core edge, where the mean tangential and axial rates of strain reach their maxima (e.g.  $z/c = -0.0436$ ), spectral levels in this frequency range are substantially lower than in the spiral wake. This could indicate that the velocity field of the vortex core may be generating little if any turbulence of its own.

Figure 22 shows the  $U$  velocity autospectrum  $G_{UU}$  measured at the core centre in the baseline flow and its evolution with distance downstream. Spectral density and

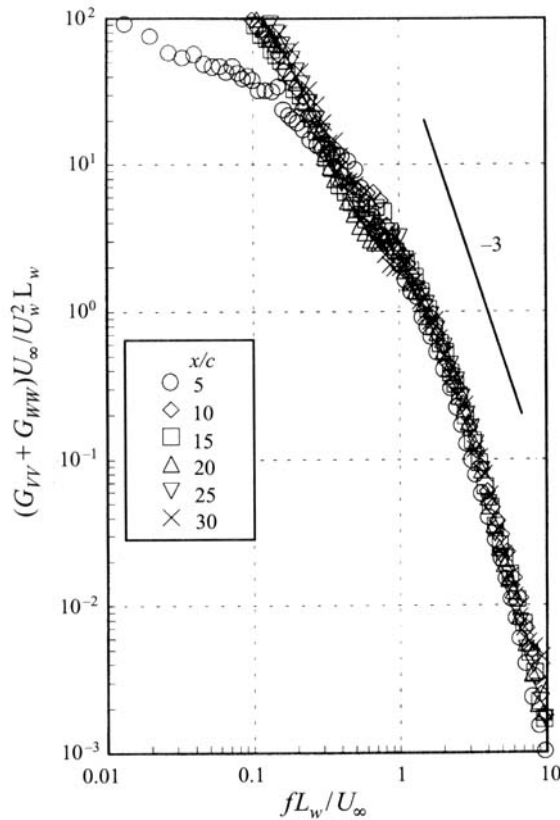


FIGURE 24.  $V + W$  spectra at the core centre in the baseline flow normalized on two-dimensional wake parameters.

frequency are normalized on the (fixed) free-stream velocity and chordlength. This figure shows a systematic shift in the spectrum to lower frequency and energy with distance downstream but little change in its shape, suggesting that the spectrum is scaling in some way. The spectra show no inertial subrange, but instead a region where  $G_{UU}$  varies approximately as  $f^{-3}$ .

To find the scaling velocity  $V$  and distance  $D$  we have replotted these spectra as  $G_{UU} U_\infty / (V^2 D)$  vs.  $fD / U_\infty$  on the presumption that the convection velocity of any disturbances should be close to  $U_\infty$ . If the velocity fluctuations in the spectrum were a consequence of turbulence generated by the rotational motion of the core we would expect  $V$  and  $D$  to be quantities that reflect the intensity and scale of the rates of strain generated by the tangential velocity field. Since the strain rate reaches its maximum just outside the core edge, the peak tangential velocity  $V_{\theta 1}$  and core radius  $r_1$  would seem to be the appropriate scales. Likewise, if turbulence were generated by the axial motion of the core we would expect the scales to be quantities such as the centreline axial velocity deficit  $U_D$  and radial scale of the axial profile  $d$ . However, normalizing on  $V_{\theta 1}$  and  $r_1$  or  $U_D$  and  $d$  or any other combination of these parameters, does not and cannot produce any collapse of the spectra in figure 22, since none of these parameters varies significantly with downstream distance. Surprisingly, the only velocity and length scales that appear to relate the core-centre spectra are those of the two-dimensional portion of the wake  $U_w$  and  $L_w$  (figure 23). Normalized on these variables  $G_{UU}$  collapses well, especially at frequencies above  $fL_w / U_\infty = 1$ . These parameters are also

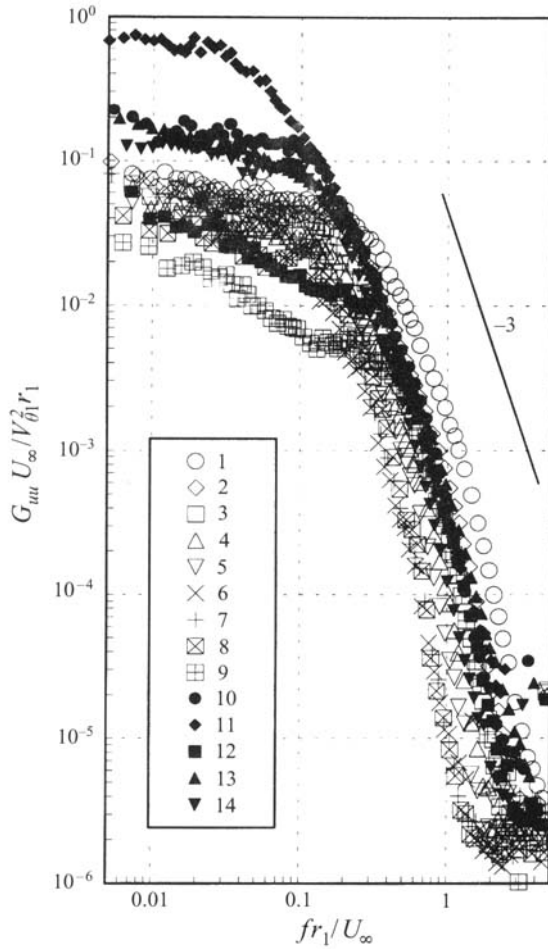


FIGURE 25.  $U$ -spectra at the core centre in all cases normalized on core parameters (see table 2 for details of the cases shown in the legend).

the only ones that collapse velocity fluctuations measured in other components, see figure 24.

This apparent dependence of velocity fluctuations in the core upon the unrolled-up portion of the wake, and independence of core parameters, is not restricted to the baseline flow. Figures 25 and 26 show  $U$  autospectra measured at the core centres for all locations in all the flows. Normalizing on  $V_{\theta 1}$  and  $r_1$  (figure 25) or other core parameters does little to relate the spectra. Normalizing on  $U_w$  and  $L_w$  (figure 26), however, produces a measure of collapse, especially between  $fL_w/U_\infty = 1$  and 3. At higher frequencies there are some differences between the normalized spectra but these appear to be associated with differences in wake Reynolds number, produced either by differences in free-stream velocity (cases 7 and 8) or trip strength (cases 12 and 13).

The fact that velocity fluctuations in the core region scale on the wake parameters would appear to imply not only the absence of turbulence generated by the core motion, but also the absence of any other turbulent motion in the core. If turbulence were present, having been diffused in from the wake, it would be stabilized to a degree controlled by the rotational motion of the core and thus would not scale. We therefore conclude that flow in the core is laminar, and that the velocity fluctuations here are the

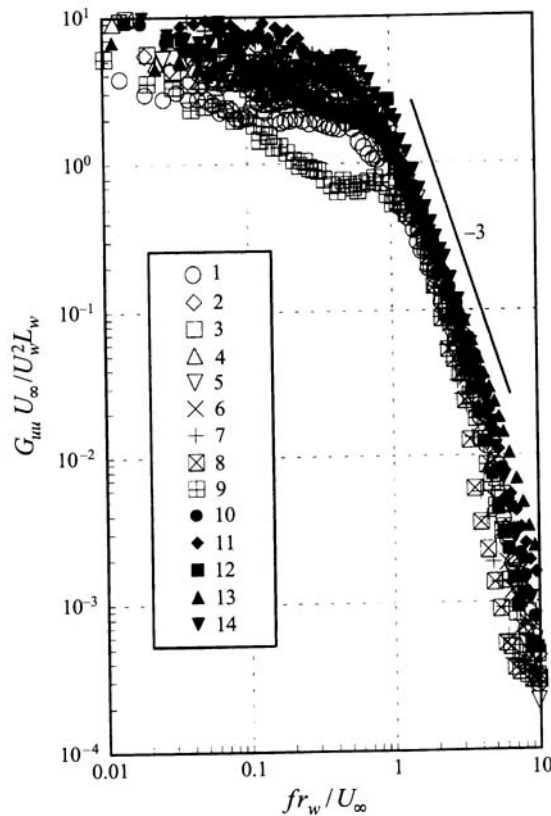


FIGURE 26.  $U$ -spectra at the core centre in all the cases normalized on two-dimensional wake parameters (see table 2 for details of the cases shown in the legend).

result of inactive motions produced as it is buffeted by surrounding (and rapidly decaying) spiral-wake turbulence. This conclusion is consistent with the development of the mean-velocity profiles, described above.

The stability arguments of Mayer & Powell (1992) provide an explanation of why the vortex core is laminar. Their results suggest that in the absence of large axial flow (i.e. for Rossby numbers  $Ro < 1$ ), trailing vortices should be stable, regardless of Reynolds number. The stability of these flows is confirmed by the large-eddy and direct simulations of Ragab & Sreedhar (1995). Their calculations also show that, even if sufficient axial flow is present to destabilize the vortex (i.e.  $Ro > 1$ ), the turbulence generated acts only to diminish the axial flow to a stable level, after which the vortex returns to a laminar state. All the present vortices are stable according to Mayer & Powell's criterion (see table 2).

The idea that the vortex shed from a turbulent-flow wing produces no turbulence and thus evolves to a laminar state may not be new, but the present study would appear to provide some of the strongest evidence to date. As discussed in the introduction, results of Cifone & Orloff (1975), Panton *et al.* (1980), Phillips & Graham (1984) and Bandyopadhyay *et al.* (1991) are also consistent with laminar flow. In Phillips & Graham's experiment, where the very slow streamwise variation in the mean-velocity fields of their case B, C and D vortices suggests viscous diffusion, significant velocity fluctuations were measured in and around the cores. Given the results of the present study we expect that these fluctuations are a consequence of inactive motion produced

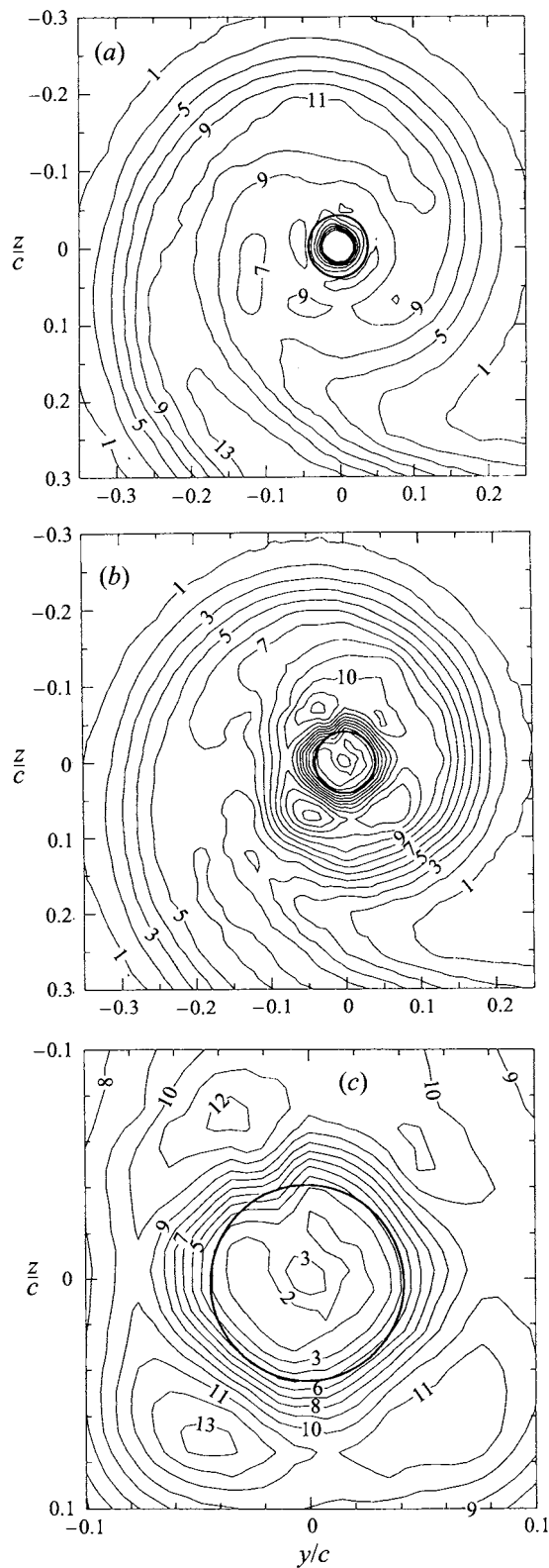


FIGURE 27. Contours of  $\overline{u^2}/U_\infty^2$  high-pass filtered at (a)  $fc/U_\infty = 3$ , (b) and (c)  $fc/U_\infty = 40$ . Contour levels multiplied by  $10^5$  in (a) and by  $10^6$  in (b) and (c). Baseline flow,  $x/c = 10$ . Thick line shows core edge.



by turbulence in the surrounding wake spiral. Indeed, turbulence stresses measured by Phillips & Graham outside the core regions show a rate of decay roughly consistent with that which would be expected of the spiral wake.

Laminar decay appears inconsistent with Phillips & Graham's (1985) case A and E vortices, and with Singh & Uberoi's (1976) and Chow *et al.*s (1994) vortices. However, according to Mayer & Powell's criterion, these flows are all unstable ( $Ro > 1$ ) or close to the stability boundary. Given Ragab & Sreedhar's (1995) work, we would therefore expect them to be in the process of evolving to a stable state via the diffusion of the axial velocity deficit. Indeed Chow *et al.* (1994) identify the axial velocity gradients as a primary source of turbulence in their vortex.

#### 4.4.2. High-pass filtering

Most velocity measurements made in the vicinity of the core were recorded at a sufficient sampling rate (50 kHz) for them to be digitally high-pass filtered during data reduction to differentiate the various sources of velocity fluctuations. In particular, at  $x/c = 10$  in the baseline flow, 'spectrally resolved' measurements of this type were made over grids of points covering the core and spiral-wake regions. Figure 27 shows these data, plotted as contours of  $u^2/U_\infty^2$  high-pass filtered at frequencies of  $fc/U_\infty = 3$  and 40, equivalent to  $fL_w/U_\infty = 0.41$  and 5.5 (see figures 23 and 24). Assuming Taylor's hypothesis, these frequencies correspond to length scales of  $0.33c$  (8.9 core radii) and  $0.025c$  (0.68 core radii) respectively.

Filtering at  $fc/U_\infty = 3$  (figure 27*a*) would be expected to eliminate most of the velocity fluctuations associated with wandering, but leave intact the bulk of fluctuations associated with coherent wake structures and inactive core motions. The flow structure appears very similar to that shown by the conventional Reynolds averaged measurements (figure 8*d*), confirming that wandering was not an overwhelming contributor to the axial normal stress at this station. Filtering does improve the definition of the innermost parts of the spiral wake, the centreline of which is visible to within about 2 core radii of the vortex centre. There is little or no axisymmetric region of turbulence surrounding the core. Inside the core, velocity fluctuations rise to a maximum presumably because of inactive motion of the core as it is buffeted by the wake.

Filtering at  $fc/U_\infty = 40$  (figure 27*b, c*) would be expected to eliminate all but the smaller turbulence scales. These contours show how the intensity of small-scale turbulent fluctuations remains almost unchanged along the outer part of the spiral wake, despite the varying rates of strain imposed by the vortex. They also show the increase in small-scale turbulence levels in the vicinity of the core. The filtered turbulence levels reach maxima in a ring between 1 and 2 core radii from the vortex centre at locations that coincide roughly with the innermost turn of the spiral seen in figure 27(*a*). Moving into the core small-scale turbulence levels drop by a factor of about 5. Inside the core stress levels are very low and almost constant, consistent with the laminar flow inferred from the spectral scaling and mean-velocity profiles above.

The ring of relatively high small-scale turbulence levels surrounding the core could be a symptom of the generation of turbulence by the rotational motion of the vortex. However, consistent with our other results, this does not seem to be the case. We can distinguish between turbulence generated by the core and associated with the spiral wake by looking at its decay rate. In the baseline flow the core radius and peak tangential velocity and the mean flow field immediately surrounding the core varied little over the 25 chordlengths measured. We would therefore expect turbulence generated by this core motion to vary little in length or velocity scale with distance

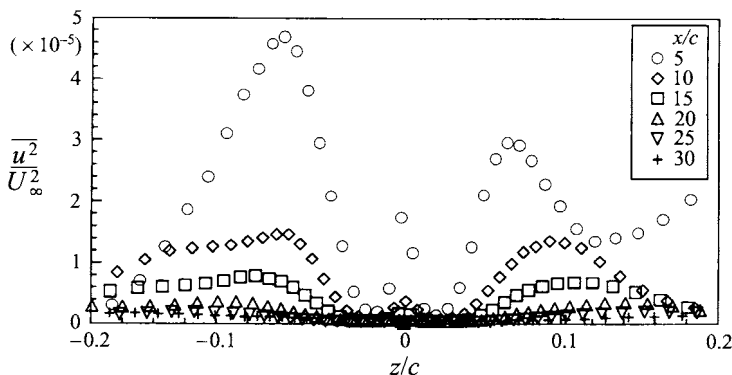


FIGURE 28. Profiles of  $\overline{u^2}/U_\infty^2$  high-pass filtered at  $fc/U_\infty = 40$  as a function of streamwise distance in the baseline flow.

downstream and thus, when high-pass filtered at a constant absolute frequency, to have a near constant intensity. Figure 28 shows profiles of  $\overline{u^2}/U_\infty^2$  through the core centre as a function of streamwise distance high-pass filtered at  $fc/U_\infty = 40$ . The low turbulence levels in the core are clearly visible at all locations downstream of  $x/c = 10$ , as are the maxima associated with the ring of higher turbulence levels surrounding the core. Turbulence levels in the ring decay very rapidly with downstream distance and show no sign of being sustained by the core. In fact, small-scale turbulence levels in the ring decay at about the same rate, or faster than, those in the two-dimensional arm of the wake. This can be seen if the profiles are filtered at a constant frequency based on wake parameters (i.e. constant  $fL_w/U_\infty$ ) and then normalizing the filtered stresses on  $U_w$ .

If the ring of elevated turbulence levels is not due to production by the vortex, then what might be its source? One possibility is that it is due to small-scale turbulence produced as the large eddies in the spiral wake are finally broken down and/or reorganized by the strong rotational motion of the vortex. The direct simulations of Melander & Hussain (1991) have shown that a line vortex can organize homogeneous turbulence into azimuthal structures. Another possibility is that it is a remnant of the initial condition. We have already hypothesized the destruction of a strong secondary vortex formed in the tip region and the redistribution of its vorticity into an annulus surrounding the main vortex as an explanation for the double core seen initially in the mean-velocity profiles. Such an event would seem likely to also generate a ring of turbulence surrounding the main vortex. Without any mechanism to sustain it this turbulence would then decay rapidly with downstream distance.

## 5. Conclusions

Experiments have been performed on the vortex shed from the tip of a rectangular NACA 0012 half-wing. Detailed measurements were made between 5 and 30 chordlengths downstream of the wing using hot-wire probes. Considerable effort was made to establish the lack of probe interference and to analyse and quantify the effects of wandering.

Wandering amplitudes were found to be small (typically less than 1% chord, 30% of the core radius). They increased with downstream distance and decreased with angle of attack, suggesting an origin in wind-tunnel unsteadiness. Careful analysis of the

effects of wandering was necessary to properly reveal the flow structure in the core region and to give confidence in measurements made outside the core. In its simplest form, this analysis yields expressions for the effects of wandering upon measured core parameters. It also shows that the velocity field of any vortex will appear as a  $q$ -vortex given sufficient wandering. In its general form the analysis provides a comprehensive method for correcting measured mean velocity profiles for the effects of wandering. The method also gives estimates of contributions of wandering to measured turbulence stress fields. Spectral decomposition was found to be the most effective method of separating these contributions from the remainder of the velocity signal.

With the wandering quantified and its effects corrected or accounted for, these measurements reveal much about the mean and turbulence structure of this flow. Outside the core region the flow is dominated by the remainder of the wake, the edge of which is wound into a spiral by the rotation of the vortex. There is no large region of axisymmetric turbulence surrounding the core and little sign of turbulence generated by the rotational motion of the vortex. The scale of the spiral  $\xi$  grows as the square root of streamwise distance. Scaled on  $\xi$ , the spiral shape appears almost constant. Outside the spiral, in the flat part of the wake, the turbulence structure of the flow appears much like that of a two-dimensional self-similar wake. Moving toward the vortex, turbulence levels initially increase from their two-dimensional values, reaching a maxima at the beginning of the spiral. They then fall as the core is approached. These variations are in response to the varying rates of strain imposed upon the wake. The wake is skewed and laterally stretched and curved by the rotating velocity field of the vortex. Some skewing of opposite sign is also produced by vorticity embedded within the wake itself, the resulting cancellation apparently producing the observed maximum in turbulence levels. Velocity spectra suggest that the additional strain rates influence the dominant large-scale turbulent motions. Small-scale motions are less affected and maintain the same absolute intensity along most of the spiral. The thickness of this part of the wake grows approximately as the square-root of streamwise distance. Since the scale of the spiral grows at the same rate, the entire turbulence structure of the spiral appears to evolve to an approximately self-similar form.

Moving from the spiral wake into the core the overall level of velocity fluctuations greatly increases, but none of this increase is directly produced by turbulence. In the frequency range likely to be associated with turbulence, velocity spectra measured at the core centre show no dependence upon core parameters. Instead, core centre spectra measured over a range of streamwise positions, vortex strengths and wake strengths collapse when scaled on the velocity and length scales of the two-dimensional portion of the wake. This implies not only the absence of turbulence generated by the core, but also the absence of any other turbulent motion. We therefore conclude that flow in the core is laminar and that velocity fluctuations experienced here are inactive motions produced as the core is buffeted by turbulence from the surrounding wake. Consistent with this, turbulence stress fields high-pass filtered to remove contributions from wandering and inactive motions show true turbulence levels to be almost constant inside the core and very low compared to those in the surrounding wake.

Velocity profiles measured through the vortex centre show little change in core parameters (core radius, peak tangential velocity and axial velocity deficit) as the flow develops. The shapes of the profiles do change, however, and at a rate that is not inconsistent with laminar diffusion. Some of the profiles, especially those measured at upstream locations, show evidence of a two-layered structure – an outer core that appears to be a remnant of a secondary vortex formed during the roll-up process and an inner core that grows within it with distance downstream.

The experimental data presented in this paper may be accessed on the World Wide Web at <http://www.aoe.vt.edu/flowdata.html>.

The authors would like to thank the Office of Naval Research, in particular Dr L. Patrick Purtell, for their support under ONR grant number N00014-92-J4087 and AASERT award number N00014-94-1-0744. The authors would also like to thank NASA Langley, in particular Dr Tom Brooks, for their financial support for early portions of this work under grant NAG-1-1119. The assistance of Mr Mark Engel during wind-tunnel testing and in providing flow visualization results is also gratefully acknowledged.

## Appendix A. The issue of probe interference

Probe interference is often cited as a serious problem in the study of tip-vortex flows. A review of the literature, however, shows that the evidence is mixed. Direct evidence that probe interference need not be a problem comes from the hot-wire/laser anemometer comparisons of Orloff (1974) and Iversen *et al.* (1979), the two-probe observations of Phillips & Graham (1984) and the flow visualizations of Stifle & Panton (1991). Direct observations of interference have been made by Mason & Marchman (1972, 1973, private communication 1994) and Green & Acosta (1991). Mason & Marchman (using the same configuration and wind tunnel as the present study) found interference only to be a problem if the probe was pitched or yawed. Green & Acosta found that even small probes could burst or displace the vortex core.

Given the uncertainty over this issue, demonstrating the absence of probe interference was an important prerequisite of the hot-wire measurements. Flow visualizations, theoretical studies and velocity measurements were carried out to this end. If present, probe interference was expected to take the form of (a) vortex breakdown propagating upstream to the measurement point, (b) waves or other disturbances travelling upstream in a laboratory frame of reference, (c) changes in core trajectory, and (d) changes the local flow field around the measurement point due to probe-generated pressure gradients.

Flow visualizations were performed by injecting helium-filled soap bubbles into the flow upstream of the wing tip to mark the vortex core. Visualizations were conducted over a large range of conditions with the present tip vortex and on pairs of counter- and co-rotating tip vortices generated in a similar manner (see Devenport & Sharma 1990; Zsoldos & Devenport 1991; and Engel 1995 for full details). The traverse gear and a dummy probe were mounted in the wind tunnel and the vortex observed with the probe in the core and traversing through it. Figure 29 shows a visualization representative of this set, taken with the probe positioned inside the vortex core with the bubbles marking the core centreline. In all the visualizations the probe had no visible effects on the vortex core at the measurement point. There was no sign of any global breakdown propagating upstream, of upstream-travelling core waves or of the probe dragging or otherwise displacing the core at the measurement point.

The absence of upstream-travelling disturbances is consistent with theoretical estimates of wave velocities. Axisymmetric, helical, bending or kink waves on vortex cores have been described by Maxworthy, Hopfinger & Redekopp (1985), Maxworthy (1988), Lundgren & Ashurst (1989), Marshall (1993) and numerous authors cited therein. We have examined the wave speed relationships quoted by these authors for all of our vortex flows. Where computing the wave speed involved approximation of the measurements, we used the most unfavourable assumptions consistent with the

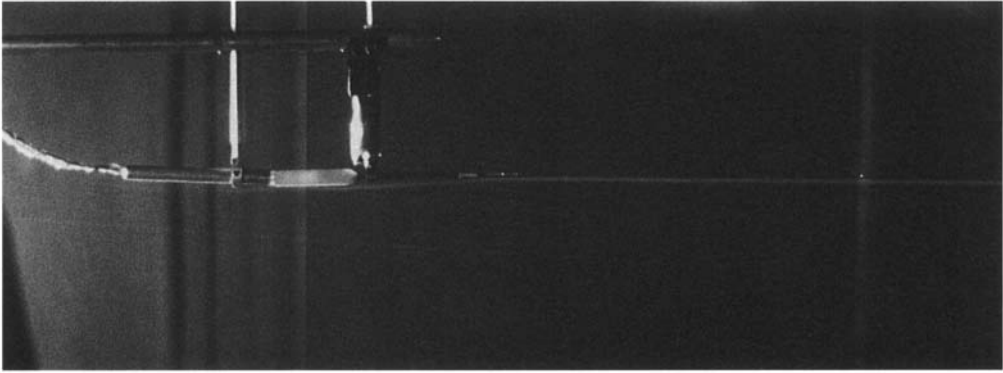


FIGURE 29. Helium bubble flow visualization showing the absence of probe interference. Flow is from right to left. Core centre is marked by helium bubble stream entering right. Core radius is slightly less than the diameter of the thickest part of the probe stem (top left). Measurement volume (centre) is therefore well inside core.

data. None of these computations indicate wave speeds greater than 60% of the free-stream velocity  $U_\infty$ , which in a laboratory-fixed frame would be swept downstream at  $0.4U_\infty$ .

A simple potential flow model of the probe was used to examine its likely influence on pressure gradients near the measurement point. The model was constructed using point sources and line doublets to represent the probe, its holder and the displacement thicknesses of their boundary layers and wakes. The pressure-coefficient gradients predicted by this model were two to three orders of magnitude smaller than the peak radial gradients associated with the vortex. The potential flow model also indicated that the flow would be decelerated by less than 0.4% in velocity at the measurement point. Further evidence that these gradients were insignificant comes in the form of velocity measurements made with a variety of probe geometries. Varying the sting diameter, length, probe type and adding a second probe to the sting displaced laterally some 2 in. from the first, produced no differences in measured mean velocities, turbulence stresses or velocity autospectra greater than the estimated uncertainty.

## Appendix B

We consider a property of a vortex flow  $g(y, z)$  that is distributed in a non-Gaussian manner. Let  $\epsilon(y, z)$  be the deviation between  $g$  and a Gaussian:

$$\epsilon(y, z) = g(y, z) - g_{GAUSS}(y, z). \quad (B\ 1)$$

In the presence of wandering we measure  $g_m(y, z)$ , that is the convolution of  $g(y, z)$  and the probability density function of vortex position  $p(y, z)$ , here assumed Gaussian:

$$g_m(y, z) = g(y, z) * p(y, z). \quad (B\ 2)$$

Let  $\epsilon_m(y, z)$  be the deviation between  $g_m(y, z)$  and a Gaussian. Then  $\epsilon_m(y, z)$  is given by

$$\epsilon_m(y, z) = \epsilon(y, z) * p(y, z). \quad (B\ 3)$$

We will show that  $g_m$  is closer to a Gaussian than  $g$ , i.e.  $\epsilon_m$  is smaller than  $\epsilon$  as a percentage of the total measured property:

$$\frac{\|\epsilon_m\|_2}{\|g_m\|_2} < \frac{\|\epsilon\|_2}{\|g\|_2}, \quad (B\ 4)$$



where  $\|\cdot\|_2$  is the usual  $L_2$  norm:

$$\|\epsilon\|_2 = \left( \int_{-\infty}^{\infty} \int_{-\infty}^{\infty} \epsilon^2(y, z) dy dz \right)^{1/2}.$$

We use the theorem (Bechner 1975) that the supremum of the expression  $\|f * h\|_r / (\|f\|_p \|h\|_q)$  with  $1/r = 1/p + 1/q - 1$  is attained for Gaussian functions  $f, h$ . We then set  $p = 2$  and  $q = 1$  which give  $r = 2$  and use this property of Gaussian functions to write

$$\frac{\|\epsilon * p\|_2}{\|\epsilon\|_2 \|p\|_1} < \frac{\|g * p\|_2}{\|g\|_2 \|p\|_1}, \quad (\text{B } 5)$$

which, after some simplifications and using equations (B 2) and (B 3), gives

$$\frac{\|\epsilon_m\|_2}{\|g_m\|_2} < \frac{\|\epsilon\|_2}{\|g\|_2}, \quad (\text{B } 6)$$

which is what we needed to show.

#### REFERENCES

- ACCARDO, L., CENEDESE, A. & CIOFFI, F. 1984 Experimental analysis of tip vortex by laser Doppler anemometry. *2nd Int Symp. on Applications of Laser Anemometry to Fluid Mechanics, Lisbon Portugal, July 2-5*.
- ANTONIA, R. A. & BRITZ, D. 1989 Phase-averaging in the turbulent far wake. *Exps. Fluids* **7**, 138-142.
- BAKER, G. R., BARKER, S. J., BOFAH, K. K. & SAFFMAN, P. G. 1974 Laser anemometer measurements of trailing vortices in water. *J. Fluid Mech.* **65**, 325-336.
- BALDWIN, B. S., CHIGIER, N. A. & SHEAFFER, Y. S. 1973 Decay of far-flowfield in trailing vortices. *AIAA J.* **11**, 1601-1602.
- BANDYOPADHYAY, P. R., STEAD, D. J. & ASH, R. L. 1991 Organized nature of a turbulent trailing vortex. *AIAA J.* **29**, 1627-1633.
- BATCHELOR, G. K. 1964 Axial flow in trailing line vortices. *J. Fluid Mech.* **12**, 645-658.
- BECHNER, W. 1975 Inequalities in Fourier Analysis. *Annl Maths* **102**, 159-182.
- BETZ, A. 1933 Behavior of vortex systems. *NACA Tech. Note* 713, pp. 237-253.
- BILANIN, A. J., TESKE, M. E. & WILLIAMSON, G. G. 1977 Vortex interactions and decay in aircraft wakes. *AIAA J.* **15**, 250-260.
- BISGOOD, P. L., MALTBY, R. L. & DEE, F. W. 1971 Some work at the Royal Aircraft Establishment on the behavior of vortex wakes. In *Aircraft Wake Turbulence and its Detection* (ed. J. H. Olsen, A. Goldberg & M. Rogers), pp. 171-206. Plenum.
- BRANDT, S. A. & IVERSEN, J. D. 1977 Merging of aircraft trailing vortices. *J. Aircraft* **14**, 1212-1220.
- BROWNE, L. B. W., ANTONIA, R. A. & CHUA, L. P. 1989 Calibration of X-probes for turbulent flow measurement. *Exps. Fluids* **7**, 201-208.
- CHIGIER, N. A. & CORSIGLIA, V. R. 1971 Tip vortices - velocity distributions. *NASA TM-62,087*.
- CHOI, K. & SIMPSON, R. L. 1987 Some mean-velocity, turbulence and unsteadiness characteristics of the VPI & SU Stability Wind Tunnel. *Rep. VPI-AOE-161*. VPI & SU, Blacksburg VA.
- CHOW, J. S., ZILLIAC, G. G. & BRADSHAW, P. 1994 Turbulence measurements in the near-field of a wingtip vortex. *ASME Forum on Turbulence in Complex Flows, Chicago IL, Nov. 6-11*.
- CIFFONE, D. L. 1974 Correlation for estimating vortex rotational velocity downstream dependence. *J. Aircraft* **11**, 716-717.
- CIFFONE, D. L. & ORLOFF, K. L. 1975 Far-field wake-vortex characteristics of wings. *J. Aircraft* **12**, 464-470.
- CORSIGLIA, V. R., IVERSEN, V. J. & CIFFONE, D. L. 1976 Experimental study of the effect of span loading on aircraft wakes. *J. Aircraft* **13**, 968-973.

- CORSIGLIA, V. R., SCHWIND, R. G. & CHIGIER, N. A. 1973 Rapid scanning, three-dimensional hot-wire anemometer surveys of wing-tip vortices. *J. Aircraft* **10**, 752–757.
- DEVENPORT, W. J., GLEGG, S. A. L. & SHARMA, G. 1992 Turbulence measurements in trailing vortices for BWI noise prediction. *Rep. VPI-AOE-192*. VPI & SU, Blacksburg VA.
- DEVENPORT, W. J. & SHARMA, G. 1990 Flow visualizations of a wing-tip vortex in the presence of a probe. *Rep. VPI-AOE-177*. VPI & SU, Blacksburg VA.
- DÖBBELING, K., LENZE, B. & LEUCKEL, W. 1990 Computer-aided calibration with a quadruple hotwire probe. *Exps. Fluids* **8**, 257–262.
- DONALDSON, C. DU P. 1972 Calculation of turbulent shear flows for atmospheric and vortex motions. *AIAA J.* **10**, 4–12.
- DONALDSON, C. DU P., SNEDEKER, R. S. & SULLIVAN, R. D. 1974 Calculation of aircraft wake velocity profiles and comparison with experimental measurements. *J. Aircraft* **11**, 547–555.
- DOSANJH, D. S., GASPAREK, E. P. & ESKINAZI, S. 1962 Decay of a viscous vortex. *Aero. Q.* **13**, 167–188.
- ENGEL, M. 1995 A wind-tunnel investigation of a wing-tip trailing vortex. MS thesis, AOE Dept, VPI & SU, Blacksburg, VA.
- FRANCIS, T. B. & KATZ, J. 1988 Observations on the development of a tip vortex on a rectangular hydrofoil. *Trans. ASME I: J. Fluids Engng* **110**, 208–215.
- GARODZ, L. J. 1971 Federal Aviation Administration full-scale aircraft vortex wake turbulence flight test investigations: past, present, and future. *AIAA Paper* 71–97.
- GASPAREK, E. P. 1957 Viscous decay of a vortex. MS thesis, Syracuse University, NY.
- GREEN, S. I. & ACOSTA, A. J. 1991 Unsteady flow in trailing vortices. *J. Fluid Mech.* **227**, 107–134.
- HOFFMAN, E. R. & JOUBERT, P. N. 1963 Turbulent line vortices. *J. Fluid Mech.* **16**, 395–411.
- HUFFAKER, R. M., JELALIAN, A. V. & THOMPSON, J. A. L. 1970 Laser Doppler system for detection of aircraft trailing vortices. *Proc. IEEE* **58**, 322–326.
- IVERSEN, J. D. 1976 Correlation of turbulent trailing vortex decay data. *J. Aircraft* **13**, 338–342.
- IVERSEN, J. D., CORSIGLIA, V. R., PARK, S., BACKHUS, D. R. & BRICKMAN, R. A. 1979 Hot-wire, laser-anemometer, and force measurements of interacting trailing vortices. *J. Aircraft* **16**, 448–454.
- KATZ, J. & BUENO GALDO, J. 1989 Effect of roughness on rollup of tip vortices on a rectangular hydrofoil. *J. Aircraft* **26**, 247–253.
- KOVASZNAVY, L. S. G. 1954 *Physical Measurements in Gas Dynamics and Combustion*, p. 227. Princeton University Press.
- LEUPTOW, R. M., BREUER, K. S. & HARITONIDIS, J. H. 1988 Computer-aided calibration of X-probes using a look-up table. *Exps Fluids* **7**, 201–208.
- LEZIUS, D. K. 1974 Water tank study of the decay of trailing vortices. *AIAA J.* **12**, 1065–1071.
- LUNDGREN, T. S. & ASHURST, W. T. 1989 Area-varying waves on curved vortex tubes with application to vortex breakdown. *J. Fluid Mech.* **200**, 283–307.
- MARSHALL, J. S. 1993 The effect of axial pressure gradient on axisymmetrical and helical vortex waves. *Phys. Fluids A* **5**, 588–599.
- MASON, W. H. & MARCHMAN, J. F. 1972 Far-field structure of an aircraft trailing vortex. *NASA CR* 62078.
- MASON, W. H. & MARCHMAN, J. F. 1973 Far-field structure of aircraft wake turbulence. *J. Aircraft* **10**, 86–92.
- MATHIOUDAKIS, K. & BREUGELMANS, F. A. E. 1985 Use of triple hot wires to measure unsteady flows with large direction changes. *J. Phys. E: Sci. Instrum.* **18**, 414–419.
- MAXWORTHY, T. 1988 Waves on vortex cores. *Fluid Dyn. Res.* **3**, 52–62.
- MAXWORTHY, T., HOPFINGER, E. J. & REDEKOPP, L. G. 1985 Wave motions on vortex cores. *J. Fluid Mech.* **151**, 141–165.
- MAYER, E. W. & POWELL, K. G. 1992 Similarity solutions for viscous vortex cores. *J. Fluid Mech.* **238**, 487–507.
- MCCORMICK, B. W., TANGLER, J. L. & SHERRIEB, H. E. 1968 Structure of trailing vortices. *J. Aircraft* **5**, 260–267.



- MELANDER, M. V. & HUSSAIN, F. 1991 Coherent structure dynamics: Interaction between large and fine scales. *8th Symp. on Turbulent Shear Flows, Munich, Sept. 9–11, Paper 28-5*.
- MERTAUGH, L. J., DAMANIA, R. B. & PAILLET, F. L. 1977 An investigation of the near-field wake behind a full-scale test aircraft. *J. Aircraft* **14**, 894–902.
- MONAGHAN, J. J. & HUMBLE, R. J. 1993 Vortex particle methods for periodic channel flow. *J. Comput. Phys.* **107**, 152–159.
- ORLOFF, K. L. 1974 Trailing vortex wind-tunnel diagnostics with a laser velocimeter. *J. Aircraft* **11**, 477–482.
- PANTON, R. L., OBERKAMPF, W. L. & SOSKIC, N. 1980 Flight measurements of a wing tip vortex. *J. Aircraft* **17**, 250–259.
- PHILLIPS, W. R. C. & GRAHAM, J. A. H. 1984 Reynolds stress measurements in a turbulent trailing vortex. *J. Fluid Mech.* **147**, 353–371.
- RAGAB, S. 1995 Direct numerical simulation of instability waves in a trailing vortex. *AIAA Paper* 95-0591.
- RAGAB, S. & SREEDHAR, M. 1995 Numerical simulation of vortices with axial velocity deficits. *Phys. Fluids* **7**, 549–558.
- REED, R. E. 1973 Properties of the lateral random oscillations of trailing vortices observed in wind-tunnel tests. *Nielsen Engineering, NEAR TR-47*, January.
- ROSSOW, V. J. 1973 On the inviscid rolled-up structure of lift-generated vortices. *J. Aircraft* **10**, 647–650.
- SARPKAYA, T. 1992 Three-dimensional interactions of vortices with a free surface. *AIAA Paper* 92-0059.
- SHEKARRIZ, A., FU, T. C., KATZ, J. & HUANG, T. T. 1993 Near-field behavior of a tip vortex. *AIAA J.* **31**, 112–118.
- SINGH, P. I. & UBEROI, M. S. 1976 Experiments on vortex stability. *Phys. Fluids* **19**, 1858–1863.
- SMITS, A. J. & KUMMER, R. P. 1985 The interaction and merger of two turbulent line vortices. *AIAA Paper* 85-0046.
- STEGER, J. L. & CUTLER, P. 1976 Implicit finite-difference procedures for the computation of vortex wakes. *AIAA Paper* 76-385.
- STIFLE, K. E. & PANTON, R. L. 1991 Experiments concerning the theories of vortex breakdown. *AIAA Paper* 91-0736.
- STINEBRING, D. R., FARELL, K. J. & BILLET, M. L. 1991 The structure of a three-dimensional tip vortex at high Reynolds numbers. *Trans. ASME Fluids Engng* **113**, 496–503.
- THOMPSON, D. H. 1975 Experimental study of axial flow in wing tip vortices. *J. Aircraft* **8**, 910–911.
- TUTU, N. K. & CHEVRAY, R. 1975 Cross-wire anemometry in high-intensity turbulence. *J. Fluid Mech.* **71**, 785–800.
- VOGEL, C. M., DEVENPORT, W. J. & ZSOLDOS, J. S. 1995 Turbulence structure of a pair of merging tip vortices. *10th Symp. on Turbulent Shear Flows, Pennsylvania State University, August 14–16*.
- VUKOSLAVČEVIĆ, P. & WALLACE, J. M. 1981 Influence of velocity gradients on measurements of velocity and streamwise vorticity with hot-wire X-array probes. *Rev. Sci. Instrum.* **52**, 869–879.
- WOOD, N. B. 1975 A method for the determination and control of the frequency response of a constant-temperature hot-wire anemometer. *J. Fluid Mech.* **67**, 769–786.
- WYGNANSKI, I., CHAMPAGNE, F. & MARASLI, B. 1986 On the large scale structures in two-dimensional small-deficit turbulent wakes. *J. Fluid Mech.* **168**, 31–71.
- ZEMAN, O. 1995 The persistence of trailing vortices: a modelling study. *Phys. Fluids* **7**, 135–143.
- ZHENG, Y. 1992 An experimental study of wing-tip vortex in the near wake of a rectangular wing. PhD dissertation, Washington State University.
- ZSOLDOS, J. S. & DEVENPORT, W. J. 1991 Flow visualizations of interacting wing-tip vortex pairs. *Rep. VPI-AOE-188*. VPI & SU, Blacksburg VA.
- ZSOLDOS, J. S. & DEVENPORT, W. J. 1992 An experimental investigation of interacting trailing vortex pairs. *Proc. 19th Symp. on Naval Hydrodynamics, Seoul, South Korea, August*.